2012-05-23

NO, Burnout, Flame Temperature, Emissivity, and Radiation Intensity from Oxycombustion Flames

Darrel Patrick Zeltner
Brigham Young University - Provo

NO, Burnout, Flame Temperature, Emissivity, and Radiation

Intensity from Oxycombustion Flames

Darrel Zeltner

A thesis submitted to the faculty of
Brigham Young University
in partial fulfillment of the requirements for the degree of

Master of Science

Dale R. Tree, Chair
Matthew R. Jones
Brent W. Webb

Department of Mechanical Engineering

Brigham Young University

June 2012

ABSTRACT

NO, Burnout, Flame Temperature, Emissivity, and Radiation
Intensity from Oxy-Combustion Flames

Darrel Zeltner
Department of Mechanical Engineering, BYU
Master of Science

This work produced the retrofit of an air-fired, 150 kW reactor for oxy-combustion which was then used in three oxy-combustion studies: strategic oxy-combustion design, oxy-combustion of petroleum coke, and air versus oxy-combustion radiative heat flux measurements.

The oxy-combustion retrofit was accomplished using a system of mass flow controllers and automated pressure switches which allowed safe and convenient operation. The system was used successfully in the three studies reported here and was also used in an unrelated study.

A study was completed where a novel high oxygen participation burner was investigated for performance while burning coal related to flame stability, NO, and burnout using a burner supplied by Air Liquide. Parameters investigated included oxygen (O_2) injection location, burner swirl number and secondary carbon dioxide (CO_2) flow rate. The data showed swirl can be used to stabilize the flame while reducing NO and improving burnout. Center O_2 injection helped to stabilize the flame but increased NO formation and decreased burnout by reducing particle residence time. Additional CO_2 flow lifted the flame and increased NO but was beneficial for burnout. High O_2 concentrations up to 100% in the secondary were accomplished without damage to the burner.

Petroleum coke was successfully burned using the Air Liquide burner. Swirl of the secondary air and O_2 injection into the center tube of the burner were needed to stabilize the flame. Trends in the data similar to those reported for the coal study are apparent.

Axial total radiant intensity profiles were obtained for air combustion and three oxy-combustion operating conditions that used hot recycled flue gas in the secondary stream. The oxygen concentration of the oxidizer stream was increased from 25 to 35% O_2 by decreasing the flow rate of recycled flue gas. The decrease in secondary flow rate decreased the secondary velocity, overall swirl, and mixing which elongated the flame. Changing from air to neat CO_2 as the coal carrier gas also decreased premixing which elongated the flame. Flame elongation caused increased total heat transfer from the flame. The air flame was short and had a higher intensity near the burner, while high O_2 concentration conditions produced lower intensities near the burner but higher intensities and temperatures farther downstream. It was shown that oxycombustion can change flame shape, temperature and soot concentration all influencing heat transfer. Differences in gas emission appear negligible in comparison to changes in particle emission.

Keywords: Coal combustion, petroleum coke, NO, burnout, flame temperature, emissivity, oxy-combustion, neat oxygen, radiation

ACKNOWLEDGEMENTS

TABLE OF CONTENTS

LIST OF TABLES

LIST OF FIGURES

1   INTRODUCTION

Clean, efficient and sustainable production of electricity is one of the most important engineering challenges our time. The most recent challenge for the production of electricity from coal is the emission of CO_2. One of several promising technologies to enable CO_2 capture is oxy-combustion. In oxy-combustion, nitrogen is removed from the oxidizer allowing a CO_2-rich product stream that is more easily liquefied, transported, and stored. This work involves the development of an oxy-fired combustion facility and use of that facility to investigate the performance of a high oxygen participation burner. Performance parameters measured included exhaust NO concentration and carbon burnout for various oxy-fired coal flames. Flame temperature and emissivity were measured to investigate the potential of oxy-firing petroleum coke. A conference paper comparing radiative heat flux intensity for air and oxy-fired coal flames is included as Chapter 0.

1.1   Energy and Coal Produced CO_2 Emissions

Coal combustion power plants are an indispensable resource for energy generation. In 2010, coal combustion was responsible for producing 45% of the electricity supply in the United States [2]. In Australia coal combustion is currently responsible for 75% of the electricity supply [3]. In 2010, 5637 million metric tons of CO_2 were emitted into the atmosphere by coal power plants in the US [2]. Other pollutants that are products of coal combustion include SO_x, NO_x, and

Mercury. Emission of these latter pollutants amounted to 5, 2, and 35 million metric tons, respectively, from coal combustion power plants in the US [4]. Aside from CO_2, nitric oxides (NO_x) constitute a major pollutant from coal-fired industrial furnaces, and must be controlled to meet government standards [5]. Ash is the mineral matter contained in coal that does not react during combustion. As long as carbon content is below 6%, ash can be used to make concrete [6].

Public concern over global greenhouse emissions has influenced the creation of international initiatives and organizations, such as the Kyoto Protocol [7] and the Intergovernmental Panel on Climate Change [8], which advocate regulations on CO_2 emission. Although renewable energy sources are a clean solution, they cannot reliably produce the amount of energy that is needed, and so the immediate energy demand is likely to be met by conventional fossil fuel combustion [9].

Current and foreseeable regulations on coal power plants have motivated extensive research on the need to decrease carbon emissions. This is because with current air combustion methods capturing the CO_2 in the exhaust is extremely expensive and inefficient. Capturing the CO_2 from an air-fired furnace is difficult because of the vast amounts of nitrogen in the mixture (80% by volume), originating in the air used as the oxidizer [9].

1.2   Oxy-Fuel Combustion

A solution that has been presented to mitigate the issue of cost and decreased CO_2 emissions is called oxy-fuel combustion. This is the simple idea of using O_2 as the oxidizer for combustion instead of air, thus eliminating the nitrogen from the system. With the oxy-fuel process, the products are mainly water and CO_2, making capture simpler and more cost-effective

[9]. A form of oxy-fuel combustion is already in use in both the glass and steel production industries [9]. In addition, oxy-fuel combustion has the potential to reduce NO_x emissions [9].

Considering oxy-fuel combustion as a retrofit technology presents many challenges in controlling the combustion environment. Changes in density, volume flow, and velocity of the fuel and oxidizer streams flowing through the burner present the possibility of poor burner aerodynamics compared to air firing, which will have an impact on ignition, flame shape and mixing [10]. Also, fluid properties such as diffusivity, density and specific heat all change with oxy-fuel combustion. This results in changes in temperature, heat transfer, reaction rates, and kinetic mechanisms that will affect flame ignition, coal burnout, emissions, and ash properties [9, 11, 12]. Current research is seeking to fully understand the implications of these changes.

1.3 Petroleum Coke

Petroleum coke, or petcoke, is a byproduct from the crude oil refining process and has high carbon content with little volatile matter [13]. Since petcoke is a waste product it is available at a lower cost than coal. Petcoke also generally has a high heating value, and has been proposed as an alternative fuel to mitigate cost and environmental constraints for power generation [14]. Fly ash in petcoke boilers has been shown to have strong adhesiveness, but research on its use in building material, as a waste stabilizer and a soil modifier is lacking [15]. However, there are many issues with petcoke that have prevented its implementation in traditional pulverized coal boilers. Lack of volatiles makes ignition difficult [13]. Also, petcoke has high sulfur, vanadium and nickel content, which results in high SO_x emissions and causes severe corrosion problems [13, 15].

One combustion process that has proven successful for petcoke for use in power generation is the circulating fluidized bed (CFB) combustor. The US is the most successful

3

country in using CFB boilers to cope with petcoke, and all of the non-CFB combustors using petcoke have been replaced by CFB boilers since 1987 [15]. However, these CFB boilers that use petcoke are continuously affected by corrosion from solid agglomerates. As a solution many CFB boilers use limestone as an additive, which acts to catch sulfur and vanadium in the ash, reducing SO_2 emissions and total corrosion [15]. Limestone as an additive has also been shown to reduce NO_x emissions [15]. CFB boilers are better able to ignite petcoke and use the limestone additive to reduce corrosion than traditional boilers. However, with oxy-fuel combustion high oxygen concentrations may lower the activation energy or raise the temperature high enough to allow petcoke to be ignited more easily in traditional coal-fired boilers.

2   BACKGROUND

In order to understand and interpret the data to be presented, a brief overview of several topics related to coal combustion will be provided. These topics include the combustion process of pulverized coal with additional discussion of NO formation and carbon burnout.

2.1   Pulverized Coal Combustion

The average pulverized coal particle is about 80 microns in diameter. It is composed of about 55% fixed carbon, 35% volatile matter, 6% ash, and 4% moisture by mass [16] although this composition can vary significantly from one coal to another. Particles are transported to the burner in a carrier gas that is normally air, called primary air. For oxy-coal combustion the carrier gas may be cleaned and dried recycled flu gas or CO_2. The primary stream of coal and carrier gas enters the boiler or reactor through the burner. The particles are heated by radiation from hot surrounding surfaces or by mixing with product gases inside the boiler. As the particle is heated, the moisture evaporates and the volatiles are released as gases. The coal particle with the volatiles removed is char. As the volatiles are heated to a reacting temperature, they will react to the extent that they are premixed with oxygen. Devolatilization and the subsequent premixed reactions are very rapid, on the order of 10 ms. After these initial premixed reactions, pockets of fuel-rich products, volatiles, coal, and char remain. The size and shape of these pockets varies depending on the burner turbulence and mixing properties. Soot forms within these fuel-rich

5

pockets. The volatiles within these fuel-rich pockets burn at the rate that the oxidizer is mixed into the fuel-rich region leaving char. The volatiles are typically produced and consumed within a few milliseconds. The remaining char oxidizes heterogeneously (solid and gas phase reactions) as oxygen is transported to the char surface, primarily by diffusion. This process is slower lasting 100 – 2000 ms. The ash is the material remaining at the end of the combustion process. The ash is composed primarily of inorganic material (silicon, alumina, and calcium). Carbon burnout refers to the fraction of the carbon remaining in the ash compared to the carbon initially in the coal.

2.2   NO$_x$ Production

There are three basic sources of NO formation: thermal, prompt, and fuel NO paths. Thermal NO formation includes the reaction of N_2, O_2, and OH at elevated temperatures (nominally above 1800 K), and is described by the extended Zeldovich mechanism [5] shown in Equations $N_2 + O \leftrightharpoons NO + N$ (2-1 through $N + OH \leftrightharpoons NO + H$ (2-3. The N_2 supplied to this process comes from the air. Prompt NO formation is caused by hydrocarbons from the fuel reacting with N_2 to form HCN as an intermediate to NO formation; and is described by the Fenimore mechanism [5] shown in Equation $CH + N_2 \leftrightharpoons HCN + N$ (2-4. Since the nitrogen for these two paths comes from air, the consensus is that the thermal and prompt NO formed in oxy-fuel coal combustion is reduced to negligible amounts [10, 11].

$$N_2 + O \leftrightharpoons NO + N \tag{2-1}$$

$$N + O_2 \leftrightharpoons NO + O \tag{2-2}$$

$$N + OH \leftrightharpoons NO + H \tag{2-3}$$

$$CH + N_2 \leftrightharpoons HCN + N \tag{2-4}$$

6

The dominant path for NO formation in coal combustion is fuel-NO. Coal contains nitrogen in both the volatile matter and in the remaining char. The nitrogen found in the coal particles is the dominant source for NO production for both air and oxy-fuel combustion [5, 11]. A mechanism for volatile fuel-NO formation is provided in Figure 2-1. Notice at the end of this mechanism flow chart the two paths to either N_2 or NO from N. If O_2 is present, there is a strong probability of NO being formed. However, if O_2 is not present NO can combine with N to form N_2, a harmless product. The key to N_2 formation over NO formation is the release and reaction of nitrogen containing species into fuel rich regions where the nitrogen can be converted to N_2 rather than NO.
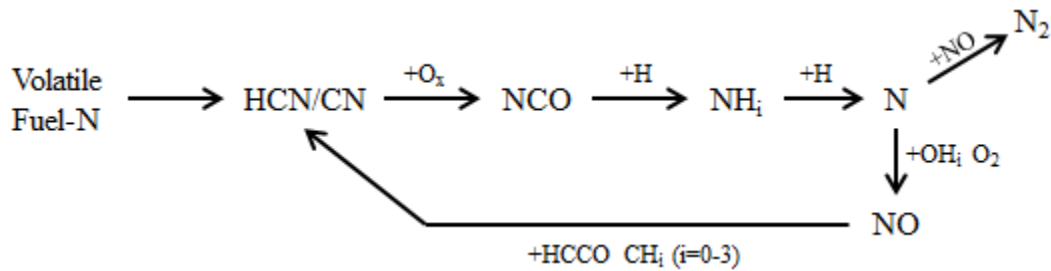
Figure 2-1: The main reaction pattern for the conversion of fuel-N to NO and N_2 [5].

One of the methods for accomplishing this is to produce a coal burner that creates a fuel-rich recirculation zone into which the primary fuel/oxidizer mixture is delivered. Recirculation zones are often created using swirl or tangential momentum in the secondary oxidizer stream. As a swirled stream leaves a burner tube into a larger volume, rotational inertia will cause the fluid to move radially outward. This expansion produces a negative pressure in the center of the swirled stream. The negative pressure creates a back flow of products below the burner up into the center of the burner where it can provide the heat necessary to release the volatiles and the fuel rich environment needed to reduce fuel nitrogen to NO. An illustration of a burner with a

7

swirled fuel stream is shown in Figure 2-2. This burner is drawn with the geometry used in experiments to be reported. The center tube was used to introduce oxygen into the reactor. The inner annulus was swirled as shown and contained the primary fuel and carrier gas. The outer annulus was used for the secondary oxidizer (in our case O_2/CO_2 mixtures). The flame boundary is highlighted with red and the recirculation zone is shaded in gray. This figure also represents the general flow field of the burner used in this work.
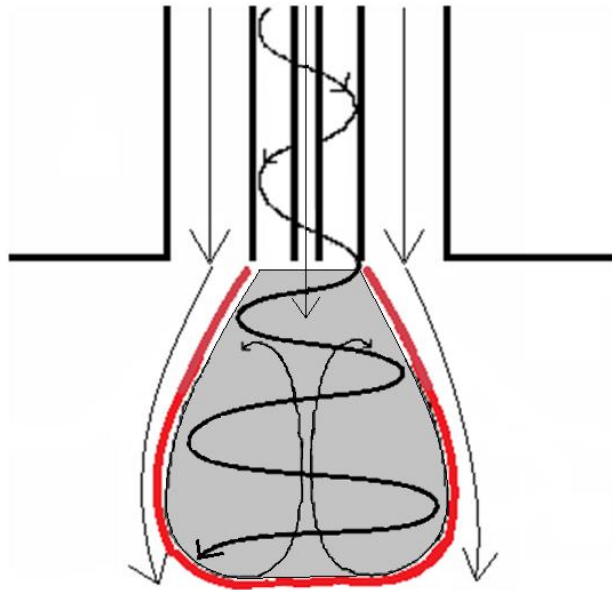
Figure 2-2: Flow field and flame boundary with primary swirl.

The swirl number is a non-dimensional parameter defined as the ratio of the tangential to axial momentum. A swirl number was calculated for each flow configuration considering all of the flows exiting each burner tube and annulus as shown in Equation $Swirl\# = \dfrac{\sum G_\varphi}{\sum G_z R}$ (2-5.

$$Swirl\# = \frac{\sum G_\varphi}{\sum G_z R}$$
(2-5)

G_φ and G_z are defined in Equations 2-6 and 2-7, respectively. In calculating these values, turbulent velocity fluctuation terms were ignored and pressure was assumed to be atmospheric. In order to evaluate G_φ and G_z, the velocity profile in the radial direction must be known. A constant velocity profile is assumed for calculations presented. A linear radial profile between tubes was also considered and compared to the constant velocity radial profile, and the difference in calculated swirl number was negligible. An important point to note for this calculation is that the swirl number changes for every different condition. For example, increasing CO_2 flow in the secondary when it is not swirled will increase axial momentum without increasing tangential momentum and thereby decrease swirl. Changing the location of O_2 injected into the burner also changed axial momentum. Changing the angle of the axial swirl is a third way the swirl number was changed.

$$G_\varphi = \int_{r_1}^{r_2} r\rho\left(u\omega + \overline{u'\omega'}\right)2\pi r\, dr \qquad (2\text{-}6)$$

$$G_z = \int_{r_1}^{r_2} \left(\rho\left(u^2 - \overline{u'^2}\right) + (P - P_\infty)\right)2\pi r\, dr \qquad (2\text{-}7)$$

Understanding the resultant flow field shown in Figure 2-2 is important in interpreting the results of this work. The shaded region shown in Figure 2-2 will be called the fuel-rich region hereafter. For swirled flows, the fuel-rich region is also a recirculation zone. Since the flame forms a boundary around this region, diffusion by O_2 is prevented because it will react with the fuel as it passes through the flame.

The char-N also contributes to NO formation, but in a more direct path. Wendt and Schulze [17] used kinetic models to investigate this path. The char particles react with oxygen heterogeneously. During this reaction, the nitrogen in the particles will form NO. Similar to volatile fuel-NO reduction discussed above, char fuel-NO reduction can occur as described by

the overall reaction in Equation 2-8 [18]. However, other factors have been shown to affect NO

formation while burning char more significantly than this reduction does such as fuel preparation

procedure, fuel type, and operating temperatures [19]. After NO is formed, its reduction in char

combustion is significantly reduced when compared to volatile combustion, as many of the

volatile compounds that help reduce NO in volatile combustion are not generally part of the

composition of char. Petcoke has about 10 wt% volatile matter, which is usually less than a third

of a bituminous coal. So while volatile combustion in the petcoke flame exists, it does not affect

NO formation as heavily. Char-N is the most significant source for NO formation in petroleum

coke flames.

$$NO + C \rightarrow \frac{1}{2}N_2 + CO, CO_2 \qquad\qquad\qquad (2\text{-}8)$$

2.3   Carbon (Char) Burnout

The term burnout, or carbon burnout, refers to the extent to which the carbon in the coal

particles has been oxidized. After devolatilization has occurred, the coal particle is composed of

carbon and mineral matter which will become ash. Energy release associated with ash oxidation

is minor, but the mineral matter in char can act as a catalyst for carbon oxidation. Char does not

react as readily as does the volatile matter, and must be subjected to the combustion environment

for a longer period of time (seconds) to fully react [5].

2.4   Flame Temperature

Strictly speaking, a flame is a thin reaction zone separating products from reactants. The

region commonly referred to as a coal flame is not a single flame at all but rather a mixture of

coal, char, ash, and radiating soot that is likely composed of many pockets of fuel-rich regions

surrounded by flames. These flame pockets or flamelets take on various shapes and sizes depending on the turbulence and mixing of the fuel and oxidizer. Soot particles are produced within pockets where the fuel mixture is heated in the absence of sufficient oxygen. Because soot particles are so small (sub-micron) they readily take on the surrounding gas temperature which may be too low on the fuel-rich side for the soot to be visible. The soot particles are most visible when they pass through a thin flame and are oxidized and heated to the flame temperature.

Radiation from soot within these flamelets dominates the emission from the near burner coal flame region [1]. The temperature measurements to be reported in this work were obtained from radiation from soot in the coal flames, which will be biased toward soot particles in the highest temperature flamelets. This means that the temperatures reported are not average gas temperatures but temperatures representing the hottest soot particles in the flame, which are at similar temperatures as the hottest gas temperatures in the flame.

2.5 Emissivity

The radiative transfer equation is given by Equation (**2-9**, where the first term on the right hand side represents extinction along the path length z, the second term represents emission and the third term represents scattering from outside the line of sight into the line of sight [20]. These terms relate to the change in spectral intensity along a line of sight, or the term on the left hand side. I_λ is the spectral intensity and z is the position along the line of sight. The function $p(\theta,\phi)$ is the phase function that represents the fraction of all scattered light into the line of sight from the polar coordinate θ and the azimuthal coordinate ϕ. The coefficients $k_{e,\lambda}$ and $k_{a,\lambda}$ are the extinction and absorption coefficients respectively, where $k_{e,\lambda} = k_{a,\lambda} + k_{s,\lambda}$.

$$\frac{dI_\lambda(z)}{dz} = -k_{e,\lambda}I_\lambda(z) + k_{a,\lambda}I_{b,\lambda} + \frac{k_{s,\lambda}}{4\pi}\int_0^{2\pi}\int_0^\pi I_\lambda(z,\theta,\phi)\,p(\theta,\phi)\sin\theta\,d\theta\,d\phi \qquad (2\text{-}9)$$

11

Assuming negligible scattering, constant temperature and constant extinction coefficient along the path length, the radiative transfer equation can be greatly simplified and solved to produce Equation 2-10. These are significant assumptions that can be a source of error, but are necessary for obtaining any sort of information.

$$I_\lambda(L) = \left(1 - e^{-k_{e,\lambda}L}\right)I_{b,\lambda} = \varepsilon_\lambda I_{b,\lambda} \tag{2-10}$$

Murphy and Shaddix [21] review this radiative transport equation in detail and discuss the errors associated with its use to determine emissivity and temperature from two-color pyrometry in flames. They point out that scattering is negligible for incipient soot particles because of their small size but not for agglomerates. Therefore, incoming and outgoing scattering are not negligible. The error in out-scattering can be somewhat quantified based on empirical measurements of scattering from laser-based measurements in flames but the in-scattering term is more difficult to quantify. In cases where the line of sight is surrounded by a thick cloud of scattering particles as is the case in coal flames, they conclude that inscattering and outscattering are similar in magnitude. Therefore the assumption is somewhat justified. The emissivity as defined by Equation 2-10 and obtained by solving this equation for two measured color bands is the emissivity reported in this work.

Draper et al. [22] describe the use of the two-color method and calibration of a two-color digital camera that was used to obtain the temperature and emissivity data for this work.

3 LITERATURE REVIEW

Motivated by the potential of oxy-coal combustion to enable the capture and sequestration of CO_2, numerous studies have been conducted over the past decade in order to provide insight into this technology. Excellent review articles on oxy-coal combustion have been completed by Buhre et al. [9], Wall et al. [23] and Toftegaard et al. [10]. Unlike the vast majority of this research, which has been focused on understanding how to retrofit existing coal-fired boilers with oxy-combustion, this research is motivated by exploring unique or new ways to utilize oxygen in the combustion process. More specifically, this research explored the use of directed neat oxygen injection at specific locations in a burner and the impact that this injection produced on NO and burnout in a coal flame and NO, temperature and emissivity in a petcoke flame. Some of the main conclusions of oxy-coal combustion relative to NO and burnout will be given, followed by a more detailed review of high oxygen participation coal flames where oxygen injection location has been explored or oxidizers of high oxygen concentration have been used. Following the oxy-coal review, a brief review of oxygen enhanced petcoke combustion will be provided.

3.1 Oxy-Coal Studies

Many studies have been performed comparing the difference in NO_x, char oxidation, and radiative properties between air combustion and oxy-fuel combustion. These studies usually

13

attempt to simulate oxygen concentration conditions that are close to air, with a maximum overall oxygen concentration of 35 vol%.

Differences in gas properties imposed on the combustion environment due to oxy-fuel versus conventional air combustion include changing bulk gas density, heat capacity, diffusivity, and radiative properties [23]. The molecular weight for CO_2 is 44 and O_2 is 32, while N_2 is 28, making the density of the gases increase overall when replacing N_2 with CO_2. Molar heat capacity for CO_2 is also higher than N_2, likewise affecting heat transfer and temperatures. The spectral absorption for CO_2 and H_2O are higher than N_2, producing higher gas phase emission. For reactivity, the rate O_2 diffusion in CO_2 is 0.8 times that of O_2 in N_2, slowing diffusion-limited combustion reactions. If not diffusion-limited, the temperature becomes the rate-limiting factor in determining reactivity. Therefore, oxy-combustion has the potential for producing a significantly different combustion process.

3.1.1 NO_x and Char Oxidation Studies

Fundamental studies have been performed by Shaddix and Molina [11] to better understand the actual effect the oxy-fuel environment has on NO_x production. They determined that increasing O_2 concentration in the presence of volatile and char matter will significantly increase NO_x production, while maintaining constant stoichiometry. For the subbituminous coal tested, nearly 80% of the fuel nitrogen was converted to NO_x in the exhaust. Also, they found that the decreased diffusivity of O_2 in CO_2 did slow NO_x production, which effectively reduced overall concentrations. But this effect of O_2 diffusion in CO_2 was only noticed at the highest O_2 concentrations tested (36% by volume).

Wall et al. [23] used a pilot-scale furnace with 27% O_2 in the hot (wet) recycled flue gas secondary stream to compare with air-fired conditions. They reported a reduction in NO_x

14

measured per energy output from air to oxy-fuel operation by about 67%. This reduction is mainly attributed to the destruction of NO_x by recirculation into reducing environments. Other studies have confirmed this [9, 10, 11, 24]. Chui et al. [24] confirmed that recirculation of flue gases causes NO_x to drop significantly, but the oxy-fuel combustion conditions showed NO_x measurements above what was observed with air combustion. O_2 participation in the secondary stream was 28 vol%.

Similar to studies on NO_x, studies on burnout for oxy-fuel applications have been mostly limited to a simple comparison between traditional air and oxy-fuel combustion. Hecker et al. [25] found that for air applications char oxidation rates were highly dependent on residence times and activation energy based on O_2 concentrations. Most oxy-fuel studies confirmed improved burnout and faster reactions with higher O_2 concentrations [10, 12, 26]. A general consensus is that 30% O_2 by mass is needed, at least, to match burnout data when compared to air at similar conditions [10, 27, 28, 29, 30]. However, at similar O_2 concentrations to air, particle temperatures for oxy-fuel environments were lower than those observed in air environments [31]. Shaddix and Molina [12] confirmed this, noting that lower particle temperatures and burning rates were observed, which were caused by slower diffusion of O_2 through the boundary layer surrounding the reacting char particle. Also, contrary to previous thought this same study found that the higher volumetric specific heat of CO_2 does not significantly influence char reactivity rates.

A possible effect of the oxy-fuel environment that is far less significant in air-fired systems is gasification reactions with the char particles. Gasification is the reaction of char with CO_2 to form CO. Saastamoinen [32] established early on that high CO_2 concentrations may increase the char-CO_2 gasification rate, and thereby increase the total combustion rate. Makino

[33] recently confirmed this, showing that at high particle surface temperatures the char-CO_2 reaction is activated and occurs in addition to the char-O_2 reaction, and the maximum combustion rate increased in comparison to the rate with O_2 alone. Rathnam [26] pointed this out and concluded that this shows that gasification reactions may be of importance in oxy-fuel applications. However, conflicting results can still be found in the literature concerning gasification in the oxy-fuel environment, and this presents a requirement for further investigation before conclusions can be made [10].

Considering all of the parameters studied, Toftegaard et al. [10] concluded that if conditions are met in a retrofit circumstance that matches the adiabatic flame temperature from the oxy-fuel to the air case, burnout will improve with the oxy-fuel case because of higher O_2 concentrations, possible gasification reactions, and longer particle residence times [34].

3.1.2 High Oxygen Participation and Neat Oxygen Injection Studies

Few studies have investigated flame characteristics using overall O_2 concentrations higher than 35 vol%. Hu et al. [35] used a low-flow (180 g/h coal) furnace to look at emissions comparisons in CO_2 and N_2 environments, and with O_2 concentrations varying between 20-100 vol%, concluding that NO_x formation continues to increase with increasing O_2 concentrations. This trend had already been shown at lower oxygen concentrations. This study did not utilize a swirled burner, and conditions were therefore less representative of what would be seen in a commercial boiler.

Nikzat et al. [36] burned coal in a 145 kW vertically-down fired reactor with a swirled burner, much like the BFR except that the inner diameter was 10 cm while the BFR is 75 cm. Their secondary stream simulated recycled flue gas with O_2 and CO_2 gases. Nikzat et al. [36] showed that increasing the equivalence ratio with oxygen concentrations between 85-88 vol% by

changing only the secondary O_2 flow rate caused burnout to decrease and NO_x formation to generally decrease. The equivalence ratio is defined as the mass of oxygen required for complete combustion of the fuel over the actual mass used. Therefore, Nikzat et al. showed that decreasing oxygen concentration decreased burnout and NO formation. This also confirms studies done with lower oxygen concentrations. This correlation is important fundamentally, but equivalence ratios above 1 are not usually seen in commercial boilers. This study also did not utilize neat oxygen injection.

Croiset et al. [37] showed that the high CO_2 environment with oxy-fuel combustion made the flame slower and decreased stability when compared to an air environment, but neat oxygen injection into the fuel region increased flame stability comparable to air. In general, high oxygen concentrations increase reaction rates and support stable combustion [10].

Krishnamurthy et al. [38] studied the effect of asymmetrical injection of neat O_2 at near-sonic velocities to obtain a sootless combustion mode. When this mode was achieved, gas temperatures and total heat fluxes were lower but more uniform, and NO_x formation was reduced compared to the flame mode with a high amount of soot formation.

3.2   Petroleum Coke Studies

Studies that investigate the use of petroleum coke for combustion are lacking in general [39]. Particularly, recent studies using petcoke in recirculated burners with oxygen enhancement are lacking. Chen and Lu [15] reviewed petcoke combustion in circulating fluidized bed (CFB) boilers, and reported that most studies that do exist focus on reducing NO_x, SO_2, and heavy metal corrosion by using limestone as an additive and fuel blends with coal. While Yuzbasi and Selcuk [14] focused on these outputs with fuel blends of petroleum coke using a non-isothermal thermogravimetric method, they also found that burnout of petroleum coke was higher in a CO_2

environment than in an N_2 environment. This shows a similar change to oxy-fuel as coal. In that study evidence of gasification reactions were also observed. Jia et al. [39] used a CFB combustion reactor for their experiments, and found that while oxy-fuel conditions lowered NO_x levels for coal, NO_x levels stayed relatively constant for petroleum coke. They also confirmed that burnout improved from air to oxy-fuel conditions.

3.2.1   Temperature and Emissivity

Since studies on temperature and emissivity for petcoke flames are also lacking, knowledge of temperature and emissivity from coal flames will be reviewed in order to correlate with petcoke flames. Draper [1] has previously analyzed the same coal flame that is presented in this work for temperature and emissivity measurements. The following information on temperature and emissivity are conclusions from that work.

Temperature was found to be correlated to the amount of diluent mixed into the fuel-rich region of the reactor. Adding diluent to a combustion reaction will lower adiabatic flame temperatures. Likewise, it was found that higher concentrations of diluents caused measured flame temperatures to drop. The sources of diluents in the reactor were the cold CO_2 supplied to the secondary stream and the products inside the reactor that had lost heat during recirculation.

Emissivity was found to decrease with increasing O_2 availability in the fuel rich region, as it is correlated to the density of soot production in the flame. Increased O_2 availability was produced by entrainment of oxidizer in the lift-off length, mixing of fuel and oxidizer streams and direct injection of O_2 into the fuel stream.

4 EXPERIMENTAL SETUP

This chapter will describe the experimental facility and operating conditions. One of the significant contributions of this work was to design, fabricate, test, and demonstrate the use of a new O_2 and CO_2 delivery system to the Burner Flow Reactor (BFR). The documentation of this system will be provided in this chapter followed by a description of the burner and operating conditions used in the experiments.

4.1 Description of the BFR Facility

A diagram of the BFR and supporting systems is shown in Figure 4-1. The system can be broken down into three sub-systems: the reactor or BFR including the burner, the fuel and gas feed and the exhaust and recycle. The recycle system was not used in this work and will not be discussed.
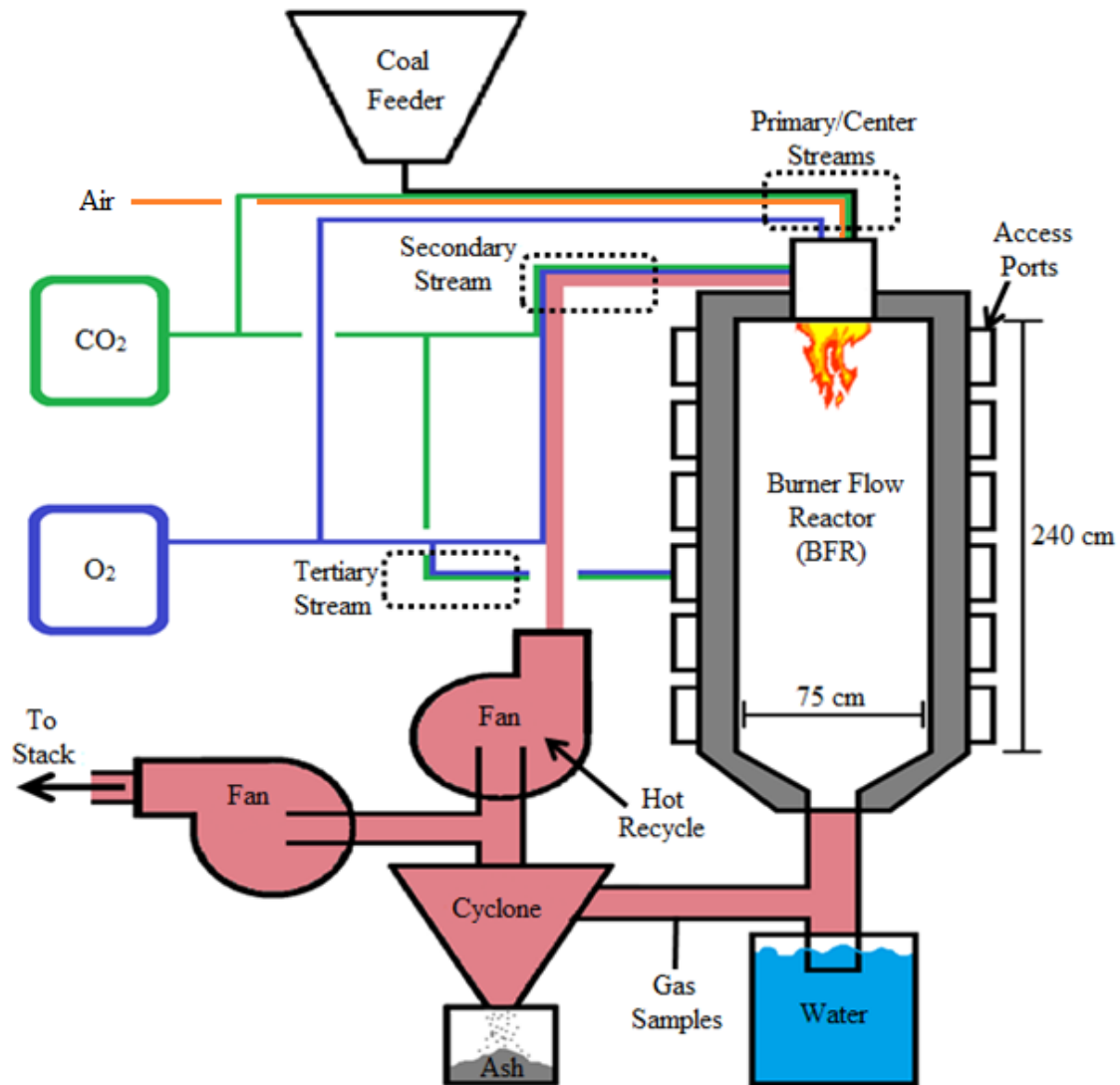
Figure 4-1: Basic schematic of the BFR and experimental system.

4.2 The Burner Flow Reactor

The BFR is a 150 kW, cylindrical, vertically down-fired reactor. The BFR consists of six

cylindrical sections each with an inner diameter of 75 cm and axial height of 0.4 m. Additional

top and bottom sections accommodate a burner and exhaust pipe, respectively. The BFR interior

is lined with refractory and then insulation, and its outer walls are water-cooled. There are four

view ports located on the north, south, east, and west sides of each section. Each view port is

rectangular with a horizontal width of 92 mm and a vertical length of 290 mm. Thermocouples are mounted flush with the inner wall on the north and south sides of each section to monitor wall temperatures. A cyclone installed downstream from the BFR exit, as shown in Figure 4-1, catches most particles above 2 μm. The exhaust system is documented by Stimpson [40].

4.2.1   The Air Liquide High Oxygen Participation Burner

The burner used in this study was designed and manufactured by Air Liquide. Exact dimensions and engineering drawings are proprietary, but the basic configuration is a pipe-in-pipe annular burner that is housed in a refractory block that contains a concentric step as shown in Figure 4-2. The primary stream where the fuel and fuel carrier gas enter the reactor is labeled as stream 2, the secondary (oxidizer) is labeled as stream 3, and an additional center O_2 injection tube is labeled as stream 1. The carrier gas for coal was CO_2 and for petcoke was air. The secondary stream consisted of various mixtures of O_2 and CO_2. The center tube was used only for neat O_2 injection. Both streams 2 and 3 (primary and secondary) have inline axial swirl inserts that can be removed or changed. The step at the bottom of the burner block was designed to produce the recirculation effect discussed in Section 2.2.

Using the dimensions of the tubes in the burner and the flow rate parameters shown in the next section, fluid velocities for each of the three streams can be estimated. Figure 4-3 shows these velocities plotted as a function of center O_2 flow rate. Since this burner had a relatively small diameter for the center stream the center velocity was in some operating conditions more than ten times the magnitude of the other streams.

21
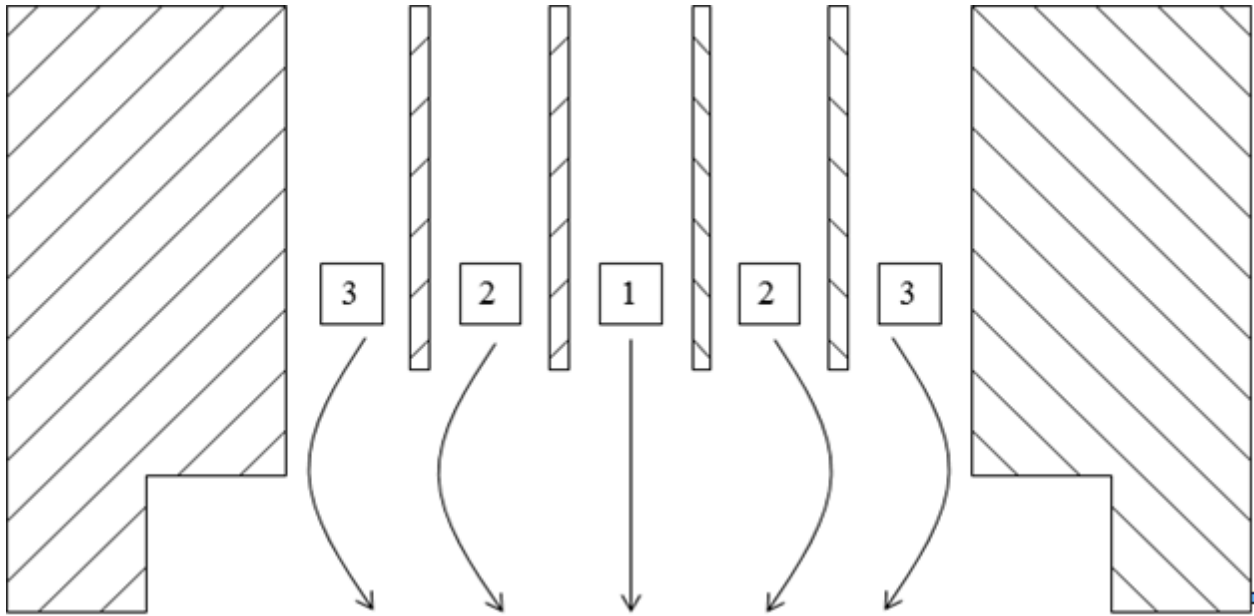
Figure 4-2: Cross-section of pipe-in-pipe, Air Liquide, oxy-coal burner.
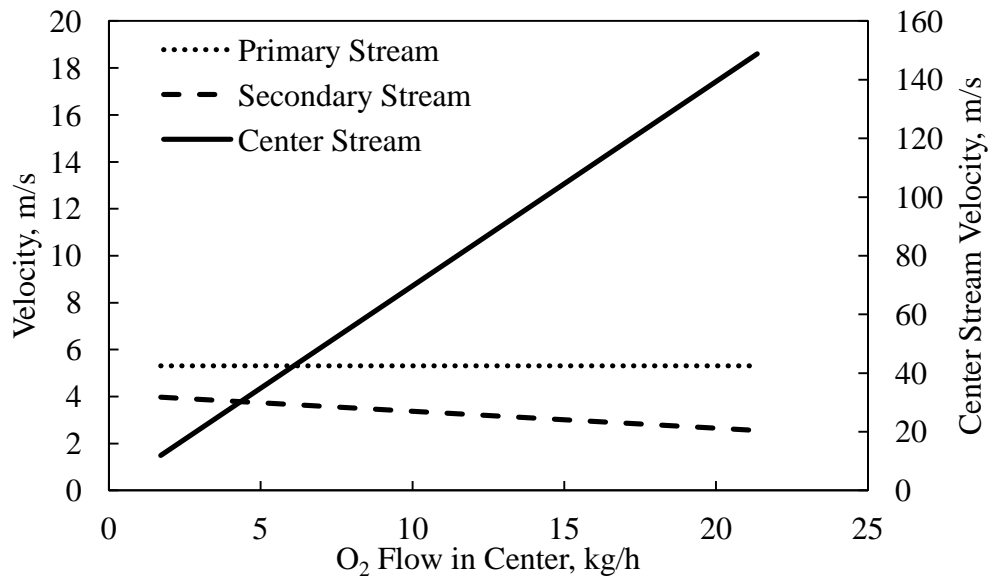
Figure 4-3: Estimated velocities for the streams exiting the burner

4.2.2 The Oxygen and Carbon Dioxide Delivery System

Previous to this study there was no CO_2 and O_2 delivery capability for the BFR. CO_2 and O_2 are potentially hazardous to the operators of the BFR. Neat oxygen is extremely reactive and should not flow through any pipe or come into contact with any material that has not been thoroughly cleaned with chemicals approved for use in environments with high oxygen concentration. If released into a room, a high oxygen concentration can start fires or explosions. Clothing exposed to oxygen is highly flammable. Carbon dioxide is primarily dangerous because it is odorless and heavier than air. If it fills an inhabited space it can cause asphyxiation. Another potential danger exists with the fuel feed system. If coal were to be delivered into a hot BFR without sufficient oxidizer, the volatiles would create an explosive mixture. For these reasons and additional safety hazards it was very important that a fuel feed system involving neat O_2 and CO_2 be designed safely. Safety design focused on redundancy of flow monitors with automated shutoff when lines were not flowing gas as desired.

Design of the delivery system was built around the gas sources and flow controls. The standard operating procedure for using this delivery system to run oxy-fuel tests on the BFR using Air Liquide's burner is found in Appendix A. Standard Operating Procedure for Oxy-Fuel

Figure 4-4 shows a schematic of both the O_2 and CO_2 storage and delivery systems, which are the sources for the gases used. Room 130 in B-41, southwest of the BFR, was made an oxygen clean-room for O_2 storage and CO_2 was stored in the fuel room in B-41, or the east annex. 250 liter liquid dewar tanks were used to supply both the CO_2 and O_2 gases. Each tank has a needle valve on the outlet labeled Liquid that flows the liquids into the system. There is also a pressure build valve on each tank that helps to control the rate that pressure builds in the tank (as the liquid gains heat and evaporates). Connections exist for two CO_2 and two O_2 dewars to allow for one dewar to remain connected and deliver gas flow continuously while the other is

being replaced. The needle valves located immediately downstream from the tanks are in place to close off flow to a single line in case only one tank is being used or if a tank needs to be replaced while running.

The vaporizer for the O_2 delivery system is a static heat exchanger, while the evaporator for the CO_2 delivery system has an electric heater. Pressure relief valves on the tanks and the delivery systems were set to open at 350 psi. If the tanks are left in the room for a time without flowing, pressure will build naturally and the valves will open periodically. This is normal, but caution was taken in making sure the oxygen clean-room remains free from material that can ignite. Also, the ventilation fan to the oxygen clean-room remained on whenever oxygen tanks were in the room. It is good practice to prevent the pressure relief valves from opening when pressurizing the delivery lines, as the liquid will sometimes freeze the valves open and continue to flow. To avoid this, the needle valve labeled Vent located on the top of each of the tanks were opened in short intervals to relieve pressure as long as the O_2 level in the room did not reach dangerous levels (alarms would go off).

Pressure regulators on each of the delivery systems shown in Figure 4-4 control the supplied pressure for the delivery systems. The pressure regulators are redundant in case of failure. The source delivery systems shown in Figure 4-4 were installed by AirGas, who also supplied the liquid dewar tanks.
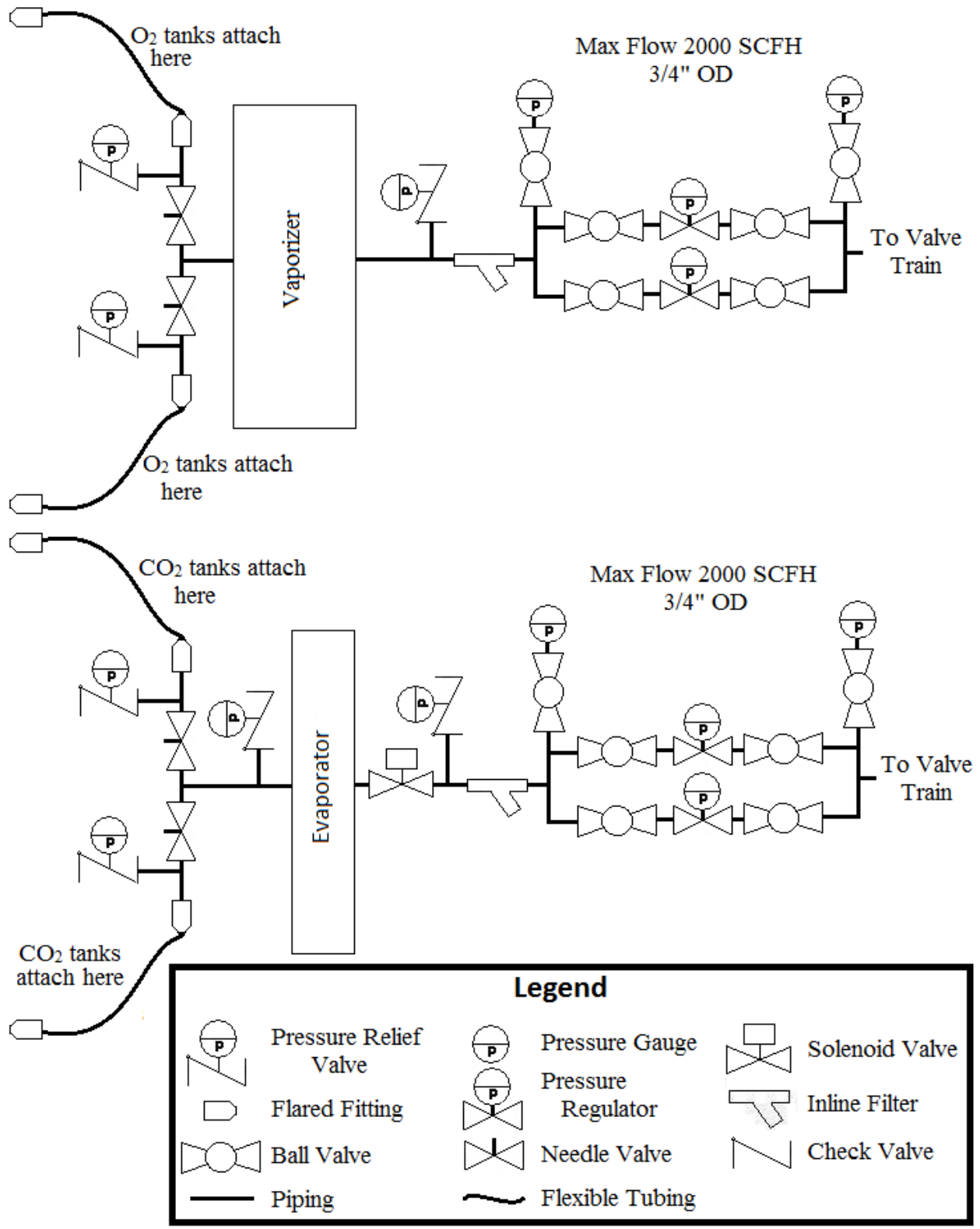
Figure 4-4: O_2 and CO_2 source schematics.

The valve train is the portion of the delivery system located on the east wall of the BFR user control area. A schematic is shown in Figure 4-5 which includes maximum flow rates and tube diameters. The gas sources supplied the valve train with a constant pressure of 80 psi for both gases. The main components of the valve train are the Alicat Scientific MCR-500SLPM-D/5M flow controllers, two for CO_2 use and two for O_2 use, labeled 11FC, 12FC, 21FC and 22FC in Figure 4-5. Although they were factory calibrated and set for O_2 and CO_2, included in their programming is calibration for other common gases, such as air, Ar, and N_2. They operate real time by controlling the opening in a solenoid valve upstream and measuring mass flow downstream based on pressure differentials across thin laminar channels. The flow controls are operated by the same LabVIEW program that monitors all the other measurements on the BFR, under the Oxy Flow tab. In order to operate the controllers using the LabVIEW program, the button on the left of the program control panel must be set to Oxy instead of Air. The communication occurs through the COM port on the computer. The COM port only allows one signal to be sent or received at a time. Sending a signal to change set points takes precedence over receiving information; and hence, when set points are updated in LabVIEW the flow controls immediately update while the LabVIEW interface has a delay in displaying the real-time measurements. These controllers supply the mass flow rates for primary and secondary CO_2 and center and secondary O_2. Caution was used with the flow controls. Maintaining a high flow set point without providing the flow potential (pressure) will cause the controlling solenoid to overheat and potentially become damaged. Thus, when flows are stopped, the set points on the flow controls were be set to 0.

For safety precautions, two manual ball valves (labeled as 10BV, 11BV, 12BV, 20BV, 21BV and 22BV) and two normally-closed solenoid valves (labeled as 10SV, 11SV, 12SV,

20SV, 21SV and 22SV) were installed on each line exiting the valve train. The ball valves were closed whenever the system was not running to protect and maintain all of the hardware. The solenoid valves were powered electrically so that if a switch was thrown, power was cut and all of the solenoid valves shut down all flows. The shut-down switch can be opened either by the manual user shut-down switch or by an automatic safety switch. The solenoid valves were powered by the circuit shown in Figure 4-6. The names for components in Figure 4-6 are also shown in Figure 4-5.

Various events were monitored for safety precautions. Probably the most common event requiring shut-down was when one of the gas supply dewars ran out of fluid. If this happened, the pressure in the depleted line dropped quickly and the flow of the other gas was maintained. If either CO_2 or O_2 flows become insufficient for combustion, the flame can go out and an excess of either fuel or neat oxygen will build up in the BFR. Both of these scenarios were unacceptable for reasons already explained. To prevent this, two low pressure switches, labeled as 10LP and 20LP, were set to open if the pressure was below 55 psi. When these switches were opened, they cut off power to the circuit powering the solenoid valves as shown in Figure 4-6. A value of 55 psi was the threshold chosen because the largest observed pressure drop in any of the lines downstream of the flow controllers was observed to be about 45 psi. A problem arose both when trying to start the reactor and when relieving the pressure in the lines, as the low pressure switches disallowed flow when the pressure was too low. In order to start up and shut down, manual override switches were installed to short the low pressure switches, and are located under the valve train on the same wall. None of the manual override switches were used while running the BFR. The low pressure switches have automatic resets, meaning that if the switch is opened

by the pressure dropping below the threshold and the pressure then rises above the threshold, the switch automatically closes again.

Another event with which precaution was taken is a surge in pressure. If the pressure regulators from the source delivery system fail, the pressure can build to dangerous levels. The valve train has a pressure rating of 100 psi. Above 100 psi components in the valve train may be damaged or fail. For this reason, two high pressure switches, labeled as 10HP and 20HP, were installed with a pressure threshold of 90 psi. These switches do not have a manual override switch, but they do have automatic resets.

Two high pressure switches, labeled as 11HP and 12HP, were installed downstream on both of the CO_2 lines. The thresholds on these pressure switches are set to 50 psi. These were used as flow switches: if there was a clog in the line hindering flow, the pressure would build and throw these switches. This precaution was to prevent flow when the flame had gone out from lack of fuel or oxidizer or to prevent pressure buildup in the O_2 or CO_2 tubing. These high pressure switches have manual reset buttons on the top, so if they were thrown the reset buttons had to be pushed in order for the switch to close again. They also do not have manual override switches. The only line that does not have flow monitored by a high pressure switch is the center O_2 stream.

Check valves were installed at the end of each line on the valve train to prevent back flow, except for the secondary O_2 line. These are shown in Figure 4-5 as a symbol with no label. The problem with putting a check valve on the secondary O_2 line is that the tubing is large, and does not provide a pressure drop downstream significant to keep a check valve open. The result was a check valve that was constantly being seated and unseated, which created pressure fluctuations that made the flow controller for that line become less accurate.

28

The last switch installed was a manual user shut-off switch. Although the emergency events discussed are monitored by automatic switches, all events cannot be predicted and complete confidence was not placed in the automatic switches to perform their designed tasks, so the BFR operator remained attentive to the operating conditions. The manual user shut-off switch is located just under the operator's window on the west wall of the user control area for the BFR. This switch was also used for system shut down after using the BFR. For diagnostic and user monitoring purposes, three pressure gauges were installed at different locations on each line of the valve train.

Stopping the coal flow was also necessary when the CO_2 and O_2 flows stopped to prevent coal buildup in the feed tube. Coal buildup causes clogging and/or energetic events. To do this, a relay was installed inside the main user control panel on the west wall in the user control area to shut off power to the feeder when power was shut off to the solenoid valves. A user switch was installed below the main user control panel to override this relay in case the BFR was being used for air-firing tests. The BFR was never used with oxy-fuel combustion when this switch was not set to Oxy-Fuel. Hence, when any of the safety switches were thrown CO_2, O_2 and coal feeds were all immediately stopped. Before restarting, it was always important to make sure the wall temperatures in the BFR were above 1000 K. If they reached below this level, reignition with methane was necessary to reheat the BFR before starting with coal again.
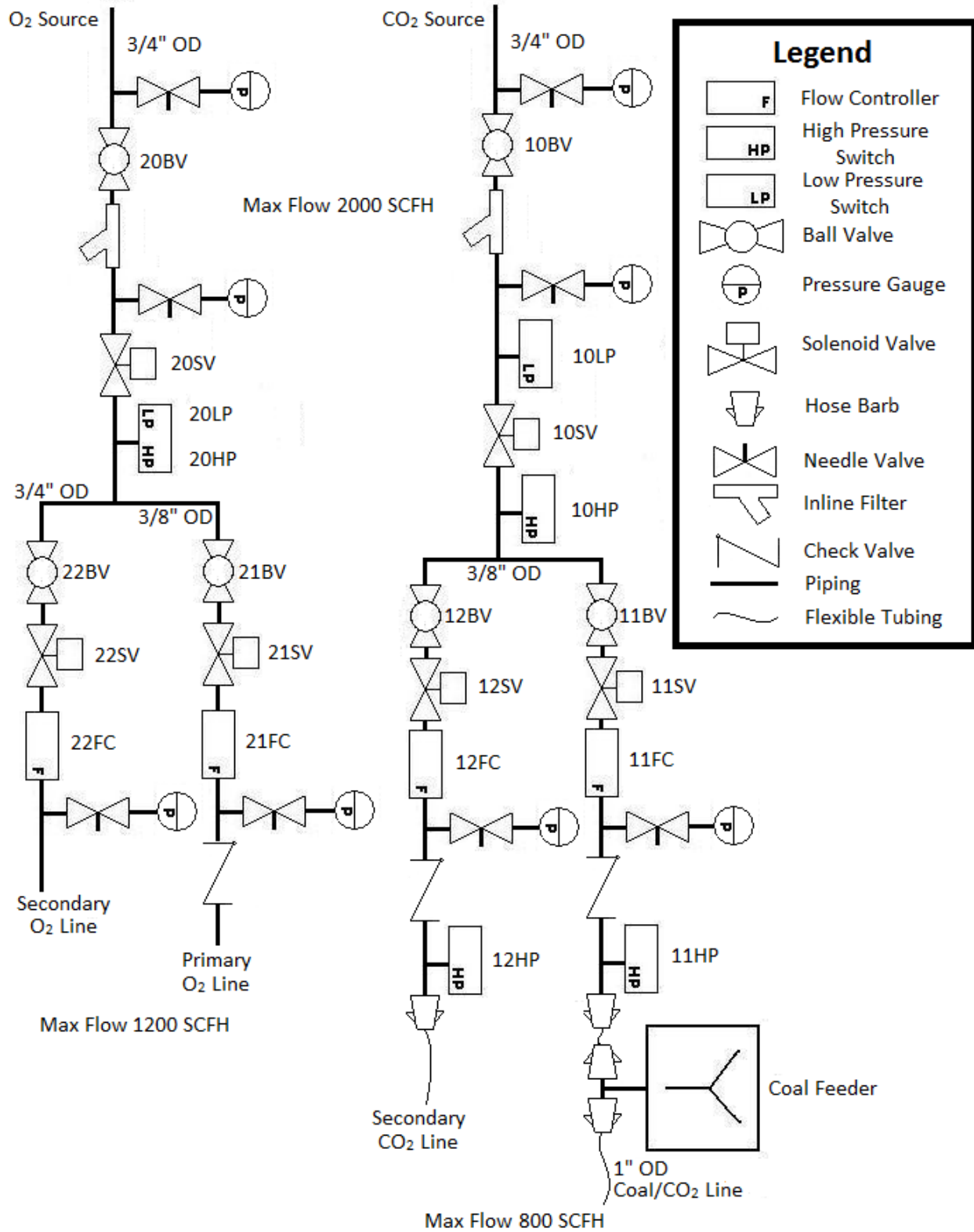
Figure 4-5: Valve train schematic.
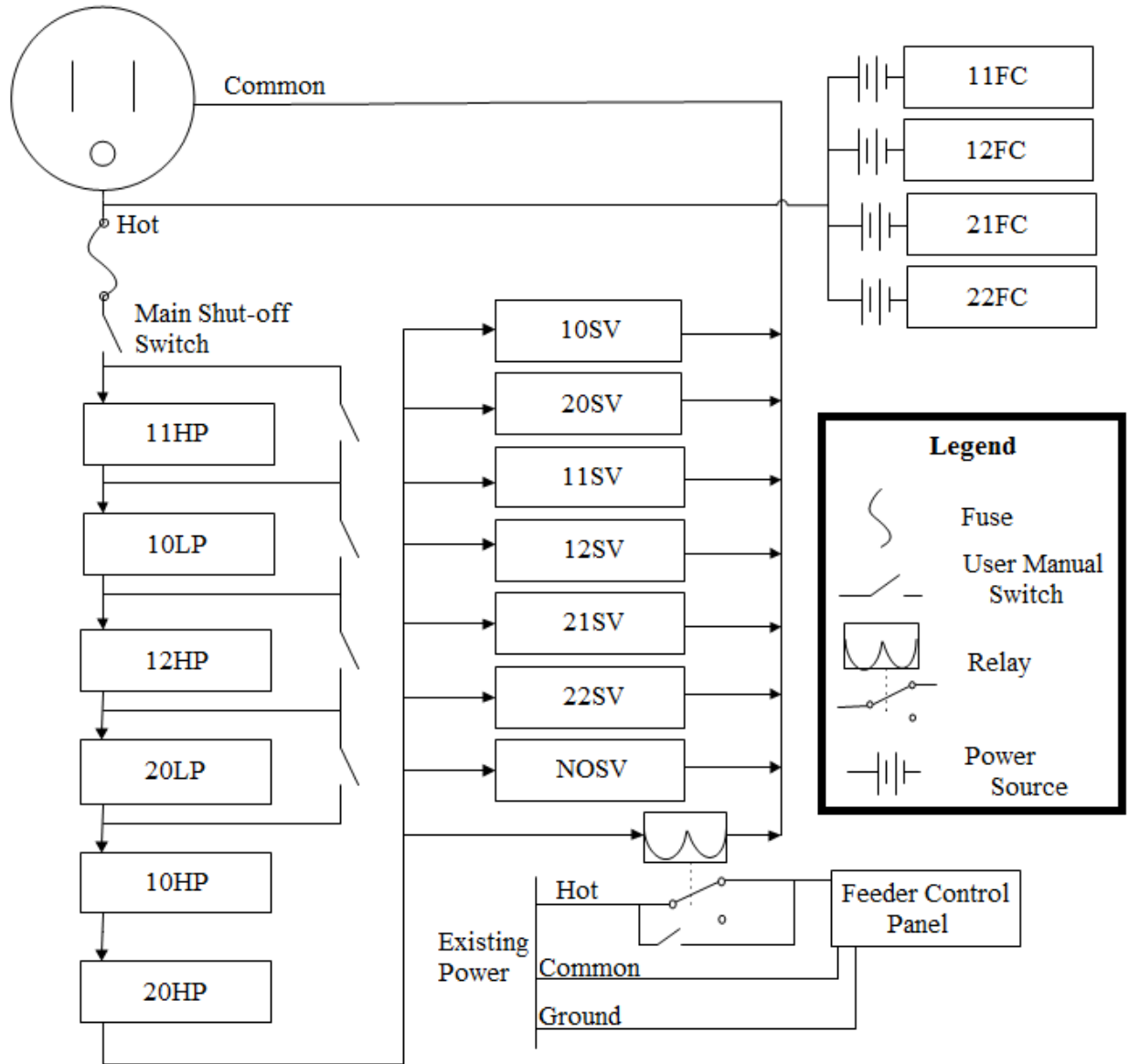
Figure 4-6: Valve train electrical schematic.

Each of the four lines leaving the valve train connect to the Air Liquide burner as shown in Figure 4-7, with lines labeled for their use and pipe and tubing sizes specified. Tubing sizes are dimensioned with an outer diameter and pipe sizes are dimensioned with an inner diameter. Ball valves prevent back flow when a line is not in use. Notice in Figure 4-7 the capability for

CO_2, O_2 and air flows into the secondary stream. The air capability in the secondary line was for heating up the BFR with natural gas. The natural gas line was plumbed into the primary line also for reactor pre-heating.

The only cooling the burner received was from the cold reactants flowing through it into the BFR. If emergency events occurred when the reactor was hot and flow was stopped, there was a risk of overheating the burner. For this purpose, an added air line is plumbed into the primary line with a normally open solenoid valve, labeled as NOSV in Figures Figure 4-6 and Figure 4-7. Thus, when power to this valve was shut off it opened while the other solenoid valves on the valve train closed. Pressure was supplied to this line by the secondary air line already installed for use on the BFR. So, when emergency events occurred, all CO_2, O_2 and coal flows stopped and air flow in the primary line started to keep the burner cool.
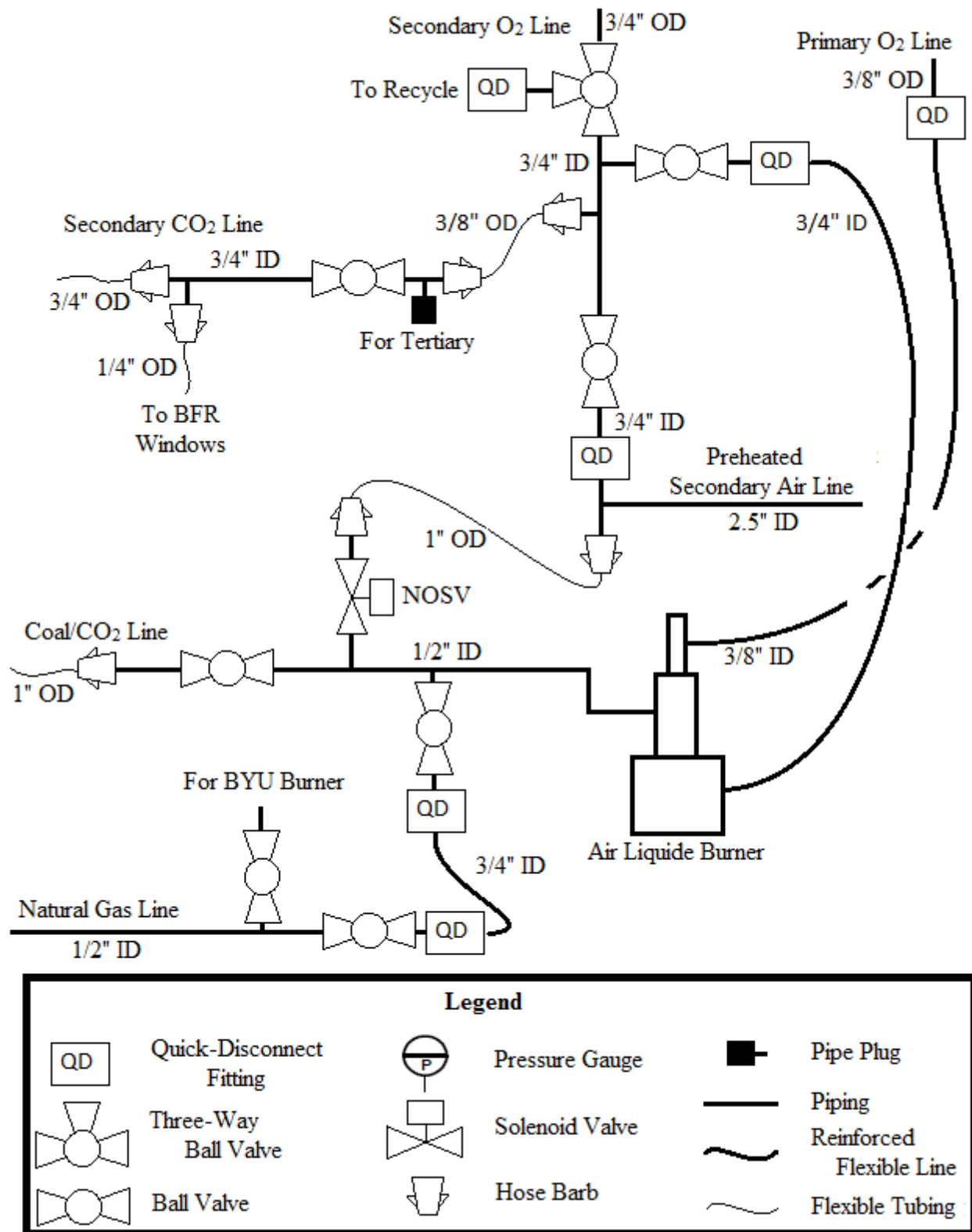
Figure 4-7: Burner connection schematic.

4.3 Fuel Parameters, Coal and Petroleum Coke

Two fuels were used in this work: a French (Flambant) bituminous coal, and petroleum coke. Compositions of both fuels are shown in Tables Table 4-1 and Table 4-2. A more extensive set of data were acquired with coal, while the work with petroleum coke was exploratory and involved only four operating conditions.

Table 4-1: Composition analysis for Flambant coal.

Analysis	Component	As Received wt%
Proximate	Moisture	3.34
	Ash	6.05
	Volatile Matter	34.64
	Fixed Carbon	55.97
Ultimate	Hydrogen	4.12
	Carbon	73.81
	Nitrogen	1.15
	Sulfur	0.90
	Oxygen	10.63
	Heating Value, Btu/lb	13,353

Table 4-2: Composition analysis for Petroleum Coke.

Analysis	Component	As Received wt%
Proximate	Moisture	0.25
	Ash	0.4
	Volatile Matter	10
	Fixed Carbon	89.35
Ultimate	Hydrogen	3.5
	Carbon	86
	Nitrogen	2
	Sulfur	6.5
	Oxygen	1.35
	Heating Value, Btu/lb	15,000

4.4 Coal Flame Operating Conditions

The objective of the coal burner testing was to explore burner performance (NO and Burnout) for a high oxygen participation burner. Parametric tests involving three parameters were investigated: swirl number, oxygen location, and secondary CO_2 addition. A list of operating conditions tested is summarized in Table 4-3.

Two different swirl vanes were used in the primary stream with angles of 15°, and 40° from vertical. Data were also taken with no swirl vane which was assumed to be zero swirl and will be labeled as such.

Total O_2 flow rate remained constant for all tests at 42.7 kg/h, but the position of O_2 was varied from 1.7 to 21.4 kg/h in the center tube in six increments, as shown in Table 4-3. 6.9% excess O_2 was used, which resulted in an average of 3.5% O_2 in the exhaust depending on the condition.

The flow rate of CO_2 in the primary used to carry coal to the burner remained constant at 25 kg/h. The amount of CO_2 delivered through the secondary stream varied from 0 to 40 kg/h in 10 kg/h increments. However, when burning coal without a swirl vane, the flame would blow out at secondary CO_2 flow rates above 20 kg/h.

Table 4-3: Flow conditions for coal.

Swirl Vane Angle (°)	Coal (kg/hr)	Total O_2 (kg/hr)	Primary CO_2 (kg/hr)	Primary O_2 (%)	Secondary CO_2 (kg/hr)	O_2 Participation Ratio (vol. %)
0	18.0	42.71	25.0	1.7, 4.3, 8.5, 12.8, 17.1, 21.4	0, 10, 20	70, 63, 57
15	18.0	42.71	25.0	1.7, 4.3, 8.5, 12.8, 17.1, 21.4	0, 10, 20, 30, 40	70, 63, 57, 52, 47.5
40	18.0	42.71	25.0	1.7, 4.3, 8.5, 12.8, 17.1, 21.4	0, 10, 20, 30, 40	70, 63, 57, 52, 47.5

4.5 Operating Conditions for Petroleum Coke

Parameters varied in the petroleum coke study included primary air flow rate (Air P), center O_2 flow rate (O_2 C), and secondary CO_2 flow rate (CO_2 S) as shown in Table 4-4. The petcoke feed rate was held constant at 16.3 kg/h. The primary stream had a 15° swirl and the secondary stream had a 45° swirl, which were both held constant for all conditions. Although swirl angle was constant, swirl changed due to the changing flow rates. Since only four operating conditions were investigated, several parameters are seen to have changed between tests, making it difficult to isolate the impact of a single variable. The carrier gas used for coal was CO_2, while the carrier gas used for petroleum coke was air in order to enhance reactivity and produce a stable flame. Also, the 45° swirl vane was used to swirl the secondary flow for these tests in order to improve flame stability.

Table 4-4: Flow conditions for petroluem coke investigated in this work.

Condition	Petcoke, kg/h	Air P, kg/h	O₂ C, kg/h	O₂ S, kg/h	CO₂ S, kg/h	Swirl Number	Total % O₂ in P
1	16.3	21.7	4	37	40	0.492	0.197
2	16.3	21.7	20.5	20.5	10	0.153	0.555
3	16.3	21.7	20.5	20.5	0	0.106	0.555
4	16.3	30	4	35	0	0.411	0.239

4.6 NO Sampling System

Gas samples were taken from the exhaust gas between the cyclone and the water barrel, shown in Figure 4-1. The sample line was cooled in an ice bucket to condense the water and sent to the gas analyzer. The analyzer used was an MKS Multi-Gas 2030 Fourier Transform Infrared (FTIR) Spectrometry gas analyzer. A discussion of the FTIR operation and uncertainty is provided by Reeder [41] and Chamberlain [42]. The output measurements of NO from the FTIR are given in dry ppm or concentration. Since the concentration of NO is impacted by the amount of inert gases independent from the conversion of fuel nitrogen to NO, the FTIR concentration was converted to an energy specific value [mg NO/MJ of fuel].

The conversion for concentration to energy-specific NO is shown in Equation (**4-1**). The dry concentration was first converted to a wet concentration (Y_{NO}). The exhaust composition and exhaust molecular weight (MW_{prod}) were calculated using the NASA Lewis equilibrium program. MW_{NO} is the molecular weight of NO, m_{total} is the total mass flow through the reactor, LHV_f is the lower heating value of the fuel, and m_f is the mass flow of the fuel. The result is an energy-specific value for NO given in mg/MJ.

$$E_{NO} = Y_{NO} * \left(\frac{MW_{NO}}{MW_{prod}} \right) * \left(\frac{m_{total}}{LHV_f * m_f} \right) \tag{4-1}$$

4.7 Ash Collection and Carbon Burnout Sampling System

Ash samples for carbon burnout measurements were obtained from the cyclone in the exhaust line shown in Figure 4-1. Ash was collected only after the reactor reached steady state, normally confirmed by steady gas species measurements and steady wall temperatures. Approximately 4 hours were required to get the wall temperatures to steady state initially, and changes between conditions were negligible. It required approximately 5 minutes to reach steady state between conditions when monitoring the exhaust gas concentrations. Fluctuations that occurred after steady state are discussed with uncertainties in Section 4.9. The ash barrel, but not the exhaust piping, was cleaned before every sample was taken. Carbon burnout was then estimated from the ash samples using the loss on ignition (LOI).

Carbon burnout is somewhat difficult to determine because oxidation of the ash produces a weight loss from other elements in the char besides carbon such as sulfur although this mass is often small relative to carbon. Measuring true carbon burnout involves measuring the CO_2 released from the oxidation of the ash. An approximation may be obtained by measuring loss on ignition (LOI) and inferring that the total mass loss is equal to the carbon mass loss. Equation (**4-2**) shows the method of obtaining LOI, where W_{dry} is the weight of the ash after it has been dried and W_{cfa} is the weight of the carbon-free ash. Equation (**4-3**) shows how burnout is calculated from LOI, where Y_{ash} is the as received weight% of ash per kg coal (see Table 4-1). This method underestimates carbon burnout but was used in this work because of its low cost and simplicity. ASTM procedure D7348 is the standard for measuring LOI using this method and was followed in this study.

$$LOI = \frac{W_{dry} - W_{cfa}}{W_{dry}} \qquad (4\text{-}2)$$

$$Carbon\ Burnout, \% = 100 * \frac{1 - Y_{ash} - LOI}{(1 - LOI) * (1 - Y_{ash})} \qquad (4\text{-}3)$$

4.8 Flame Temperature and Emissivity Measurements

Flame images were collected through the top port in the BFR, as shown in Figure 4-1. These images were captured using a UNIQ, UC-600CL, 10-bit, RGB, CCD camera looking up at the burner base. The camera was calibrated for absolute intensity measurements for each of the three colors and used to obtain two-dimensional temperature and emissivity maps of the flames as described by Draper [1]. Temperature and emissivity data for coal has been presented for this work by Draper [1], and will not be shown herein. Temperature and emissivity data will be shown for petroleum coke results.

4.9 Uncertainty in Measurements

Three different types of uncertainty sources are discussed that occurred in experimentation for this work. Precision error refers to a range of possible values that is uncertain because of resolution or variance in instrumentation. Bias error refers to a constant offset error that is uncertain because of instrumentation or calibration error. Bias error contributes to the uncertainty of absolute values of the data, but since it is a constant offset it has no effect on the uncertainty of trends. Operating variability refers to the error in repeatability of experimentation results due to the error and fluctuations in the experimental system. Operating variability has two parts: fluid flow fluctuations and block, or day-to-day, repeatability. The

combination of the precision error and operating variability gives the total error for resolving trends in the data.

The largest source of operation variability in tests performed with the BFR come from the fuel feeder. The fuel feed pulsates and often has a significant bias error. The controller for the fuel feeder varies the power to a motor that turns two screws. Those screws push the pulverized fuel into the low pressure region of a Venturi that carries the fuel to the BFR. The controller changes the power based on the change in weight that is registered in the hopper holding the fuel. The controller can average weight loss over different periods. The longer it takes to average the fuel flow rate, the less responsive the feeder can be to changes in the flow.

Assuming flow were calculated every second, at 18 kg/h, or 0.005 kg/s, the scale has to accurately read a difference in weight of about 0.005 kg with a total weight of 30-50 kg including the coal and hopper. Vibrations from surrounding machinery or construction can cause fluctuations in the scale greater than this amount. The controller therefore attempts to measure over longer periods, such as 10 seconds to a minute. Unfortunately, pressure fluctuations in the BFR and variations in the density of coal in the hopper create fluctuations in feed rate independent of auger speed over these longer time scales. Thus the steady feeding of coal is problematic, and the operation variability associated with the coal feed rate contains precision and bias error.

The other input for the BFR is the gas flow. The gas flow controllers used were made and calibrated specifically for O_2 and CO_2 flow by Alicat Scientific. The manufacturer claims an error in mass flow measurement of 0.6%. This accuracy was confirmed in-house by comparing the mass flow controller readings with a different volume flow meter located on the same line downstream. Therefore, strong confidence has been placed in the accurate and steady flow of

gases into the BFR. The fuel feed rate is the dominant source of variation in the flows into the BFR.

The developed method to correct the bias error associated with the fuel feed was as follows. Equilibrium calculations were performed to predict the feed rates for both fuel and gas flows assuming complete combustion for a desired exhaust oxygen concentration. When running the BFR, these flow rates are used initially. Assuming complete combustion, the real-time exhaust oxygen concentration is monitored. It was observed that the exhaust conditions were generally too fuel rich. The fuel feed set point was modified manually until the predicted exhaust oxygen concentration was achieved. The decrease in flow rate was typically on the order of 5%.

One way to estimate the precision error associated with the coal feed is to determine the change in coal flow rate based on the fluctuations in the exhaust oxygen concentration, and then the change in NO, burnout, temperature and emissivity produced by the change coal flow rate. Rather than predict this value, the variation in the measurements themselves can be used as an estimate. Using the variation in the measurements themselves, the total operation variability can be determined rather than just the operation variability due to the coal feed.

Since burnout data is represented as a percentage as will be errors, nomenclature is here defined. Absolute error is defined in terms of the unit of measurement (i.e. % carbon burnout, mg/MJ NO). Relative error is defined as a percentage of the unit of measurement. The average standard deviation for NO data for coal and petroleum coke tests was 1.9 mg/MJ absolute. The average standard deviation for burnout for coal tests was 0.18% carbon burnout absolute. The average standard deviation for flame temperature for petroleum coke tests was 10 K absolute. The average standard deviation for emissivity for petroleum coke tests was 0.02 absolute. Two

standard deviations are used to estimate the amplitude of error caused by fluctuations in the BFR. This results in the operational variability from flow fluctuations shown in Table 4-5.

Another source of error was the block repeatability of reactor conditions. It is known that reactor wall temperature affects flame lift-off, flame temperature and other performance parameters. The BFR can take hours to reach complete thermal equilibrium. Therefore, day-to-day repeatability is also an issue defining measurement uncertainty. Unfortunately, because of the high expense of obtaining data there was only one NO measurement that was repeated on three separate days. The resulting error from repeatability of this point was ±2.5% relative energy specific NO.

Maximum precision error was estimated by Chamberlain [42] to be ±3% relative for NO measurements, which was mostly attributed to interference of spectral bands by various gas species in the mixture. Precision error in burnout results was caused by the resolution in the scale used to analyze the ash, which related to an absolute error of ±0.005% carbon burnout, which is insignificant. Precision error for temperature and emissivity were not found, but are assumed to be negligible.

Draper [1] estimated the bias error associated with the using the camera and calculation methods used to be 147 K for temperature and .072 for emissivity. Bias error for NO and burnout measurements were not found, but are assumed to be negligible.

The uncertainty in random error is sufficient to determine trends in the data. Therefore, the total random error has been estimated from the root mean square of the three random error sources: precision error, flow fluctuation and block repeatability. The total error has been estimated from the root mean square of all error sources, and should be used when considering the absolute accuracy of the data. Table 4-5 summarizes the uncertainty discussed in this section.

Table 4-5: Summary of uncertainty associated with measurements taken.

Measurement	Precision Error	Bias Error	Operation Variability: Flow Fluctuation	Operation Variability: Block Repeatability	Total Random Error	Total Error
NO	±3%	N/A	±1.4%	±2.5%	±6.9%	±2.4%
Burnout	±0.005%	N/A	±0.36%	N/A	±0.37%	±0.21%
Temperature	N/A	147 K	±1.1%	N/A	±1.1%	±2.1%
Emissivity	N/A	.072	±7.4%	N/A	±7.4%	±8.1%

5   COAL RESULTS

Results for NO and carbon burnout are presented in this chapter for coal tests performed. Before presenting these results, flame-lift off results presented by Draper [1] will be reviewed because they are useful for explaining the trends observed with NO and burnout.

5.1   Flame Lift-off

Flame images reported by Draper [1] were obtained for the same operating conditions as the NO and burnout data reported here. The flame imaging data that is useful for interpreting the NO and burnout data will be reviewed here. Recalling the test matrix presented in Table 4-3, the three operational variables tested were: 1) swirl vane angle, 2) oxygen injection location, and 3) secondary CO_2 flow rate.

Table 5-1 shows flame images taken for three different swirl vane angles at constant secondary CO_2 flow rate of 20 kg/h and center O_2 flow rate of 12.8 kg/h. For all images presented, the burner exit is located at the top of the image, and is visible in the 40° image in Table 5-1 as the dark boundary above the flame. This sequence shows that the flame became more attached as the swirl vane angle was increased. Swirl induces a radial velocity that expands the diameter of the fuel jet upon exiting the burner. This radial component produces a negative pressure in the middle of the swirled stream that causes back flow towards the root of the flame. The resulting flow field is illustrated in Figure 2-2.

Table 5-1: Flame lift-off caused by swirl angle for 20 kg/h secondary CO_2 and 12.8 kg/h center O_2 [1].
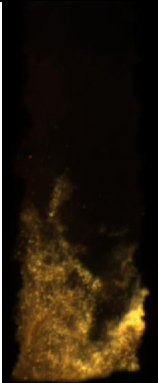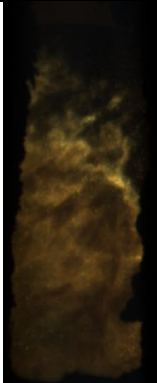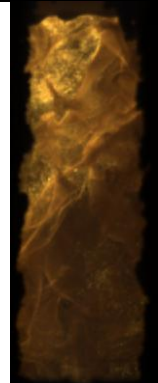
Swirl Plate Angle	0°	15°	40°
Flame Image			

Table 5-2 shows three images of coal flames with increasing center O_2 flow rate while secondary CO_2 flow rate (40 kg/hr) and swirl vane angle (15 deg.) were held constant. The addition of center O_2 is seen to have decreased the flame length and attached the flame.

Table 5-2: Flame images varying center O_2 flow rate with 40 kg/h secondary CO_2 [1].
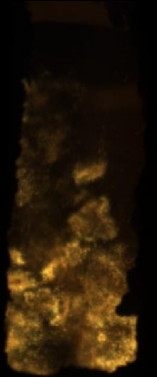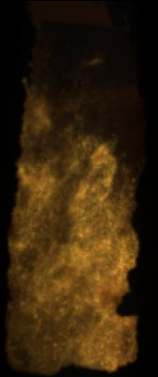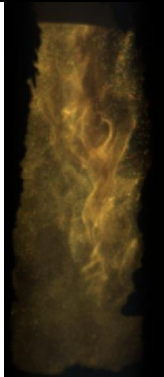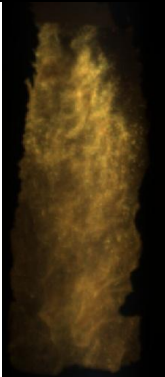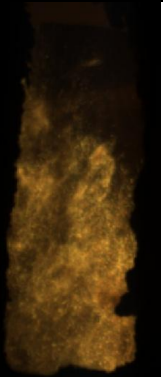
O_2 Flow in Center, kg/h	1.7	12.8	21.4
Flame Image			

Table 5-3 shows three images of coal flames with increasing CO_2 flow rate, while center O_2 flow rate and swirl vane angle were held constant. The increasing flow rate is seen to increase the lift-off length and cause increased flame detachment.

Table 5-3: Flame images varying secondary CO$_2$ flow rate with 12.8 kg/h center O$_2$ [1].

CO$_2$ Flow in Secondary, kg/h	0	20	40
Flame Image			

The lift-off length was quantified by Draper [1] by correlating pixels in the image with known distances. Figure 5-1 is a plot of lift-off length as a function of O$_2$ flow rate and CO$_2$ flow rate with the 15° swirl vane presented by Draper [1]. Notice that liftoff decreases with increasing O$_2$ flow rate and increases with increasing CO$_2$ flow rate as observed in the images. Center O$_2$ flow injects O$_2$ directly into the fuel rich region, mixing fuel and oxidizer. This enables ignition and allows for the flame to become more attached. As CO$_2$ flow rate was increased, velocity of the incoming secondary fluid increased. This could increase lift-off for two reasons. The cold CO$_2$ provides additional mass that must be heated before the coal oxidizer mixture ignites, thus delaying ignition. Additionally, the incoming CO$_2$ has no tangential momentum causing an overall decrease in swirl number, this decreases the strength of the recirculation zone which is needed to stabilize the flame.

So, increasing swirl and increasing O$_2$ flow rate attach the flame to the burner while increasing CO$_2$ flow rate detaches the flame. When the flame is lifted, the secondary stream can become entrained into the fuel rich region in the area between the burner exit and the flame ignition location. This is illustrated in Figure 5-2 where the red curve represents the flame.
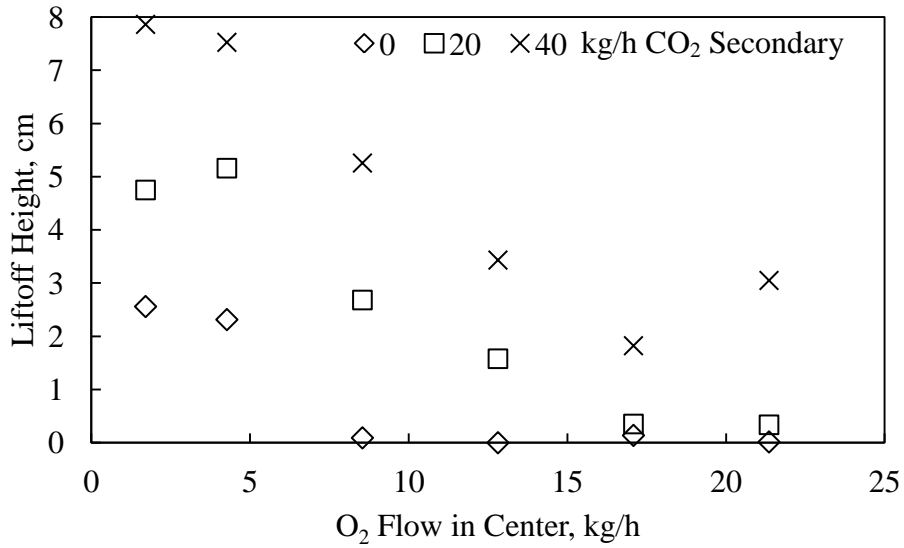
Figure 5-1: Flame lift-off length as a function of O_2 flow rate for selected CO_2 flow rates using the 15° swirl vane [1].
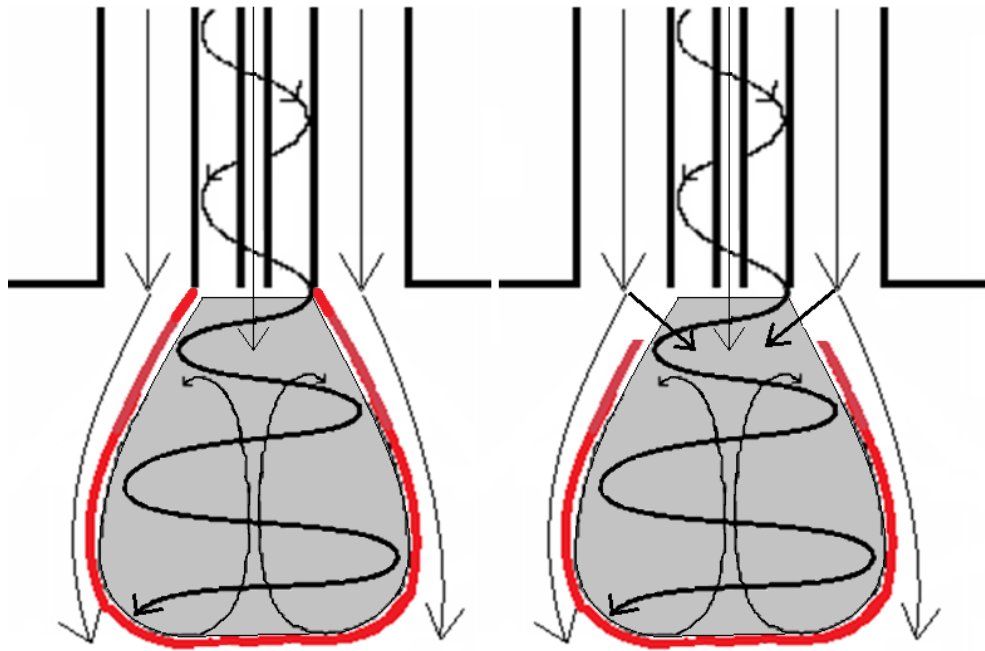
Figure 5-2: Illustration of an attached (left) and lifted (right) flame.

There was one adverse effect of swirl reported by Draper [1] that affects data obtained for the case with 40° swirl vane. Using the images of the flame and visual confirmation, it was

concluded that the high radial momentum of the primary stream caused coal to be transported radially through the secondary oxidizer flow before completely reacting. Although the flame was attached for all conditions tested with the 40° swirl vane, black clouds of coal particles were observed to protrude periodically or on one side of the flame making the flame appear unstable.

5.2 NO Measurements

NO measurements are shown and discussed as a function of the three burner parameters of interest: swirl, O_2 location, and CO_2 flow rate.

5.2.1 NO as a Function of Overall Burner Swirl Number

Figure 5-3 shows the measured energy specific NO in the exhaust as a function of calculated swirl number with the 15° and 40° swirl vanes for all tested flow conditions. The energy specific NO is seen to decrease with increasing swirl. This trend has been reported previously in the literature for air- and oxy-fuel flames [5, 24, 43]. The reduction in NO with increasing swirl is attributed to the swirl producing a stronger recirculation zone with a more attached flame. This means less oxygen entrainment into the fuel rich region where NO is reduced to N_2 as discussed in Section 2.2. An error bar has been added to a single data point representing the total random error as discussed in Table 4-5. The error bar was placed on the point of largest uncertainty. The error bars on all other points are of similar magnitude, but were not included to provide clarity for identifying individual data points. This practice of showing representative error bars is repeated in all subsequent plots.
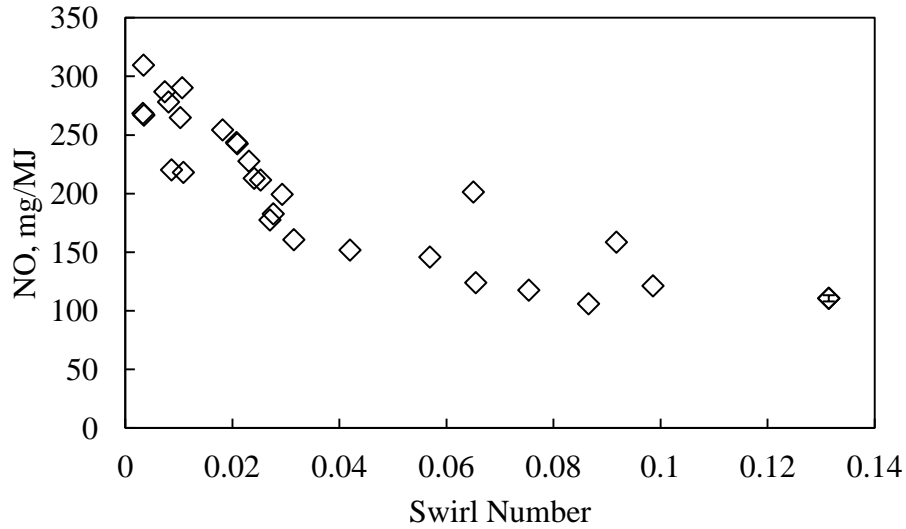
Figure 5-3: Effect of swirl number on NO with maximum error shown on data point with highest swirl.

5.2.2 Impact of Center O_2 Flow Rate and Secondary CO_2 Flow Rate on NO Emissions at Zero Swirl

Figure 5-4 shows the energy specific NO at zero swirl as a function of center O_2 flow rate and secondary CO_2 flow rate. A distinct trend of increasing NO with increasing O_2 flow rate is apparent. While the various CO_2 flow rates appear to be grouped together, closer examination shows that in most cases higher CO_2 flow rates produced higher energy specific NO. Exceptions to the trends are seen only at the highest O_2 and CO_2 flow rates.

The increase of O_2 flow rate adds oxygen to the fuel rich region where fuel volatiles containing nitrogen are released from the coal. The increased availability of oxygen in this fuel rich region increases NO formation. The increase in CO_2 flow rate increases flame lift-off and thereby increases entrainment of the secondary stream into the fuel-rich region. The O_2 carried in the secondary stream provides more oxygen for the formation of NO. At the highest secondary CO_2 and center O_2 flow rates, the secondary flow being entrained was lower in O_2 concentration

50

and therefore may not have been as effective at forming NO. The data showed that increasing O_2 flow rate affects NO formation more significantly than does increasing CO_2 flow rate.
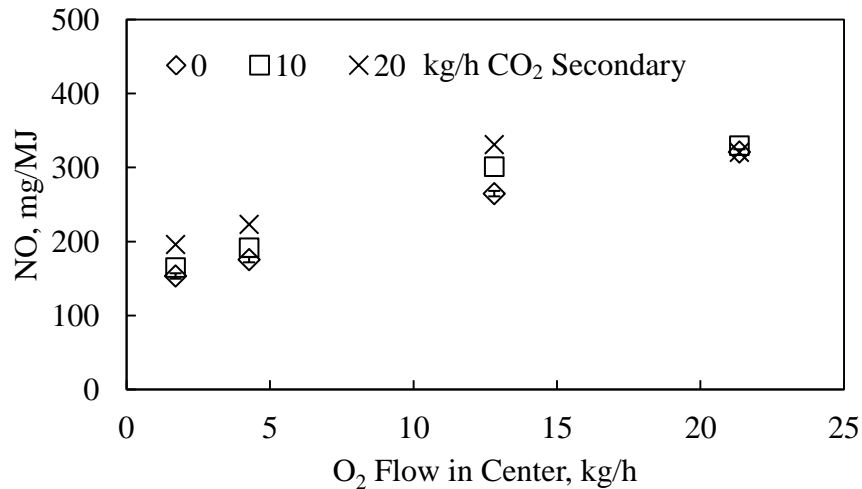
Figure 5-4: Effect of O_2 location and CO_2 dilution on energy specific NO with no swirl with maximum error shown on 0 kg/h CO_2 series.

5.2.3 Impact of Center O_2 Flow Rate and Secondary CO_2 Flow Rate on NO emissions with the 15° Swirl Plate

Figure 5-5 shows a plot of energy specific NO measured as a function of O_2 flow rate and CO_2 flow rate. The trends obtained were almost identical to those shown in Figure 5-4. Energy specific NO generally increases with increasing O_2 flow rate and with increasing CO_2 flow rate. The exception is again at 21.1 kg/h center O_2 flow rate, where energy specific NO drops with 40 kg/h CO_2 flow rate. Again, the results in Figure 5-5 show that increasing O_2 flow rate will increase NO formation in the fuel rich recirculation zone, and increasing CO_2 flow rate will increase entrainment of O_2 in the secondary stream into the recirculation zone with the same effect. Although, with the 15° swirl plate, increasing CO_2 flow rate has more effect on NO formation than without swirl.

51
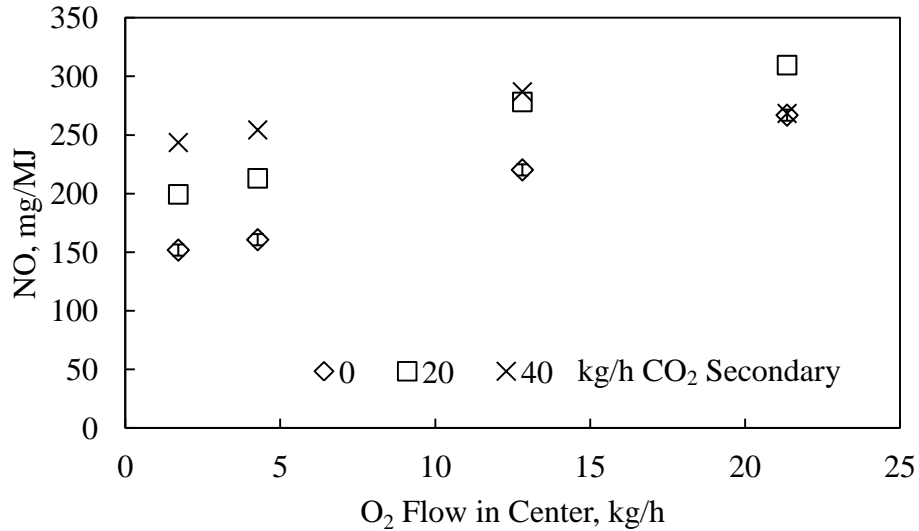
Figure 5-5: Effect of O_2 location and CO_2 dilution on energy specific NO with 15° swirl with maximum error shown with 0 kg/h CO_2.

5.2.4 Impact of Center O_2 Flow Rate and Secondary CO_2 Flow Rate on NO emissions with the 40° Swirl Plate

Figure 5-6 shows energy specific NO measured as a function of O_2 flow rate and CO_2 flow rate using the 40° swirl vane. These data show mostly the same trends as seen when using the zero and 15° swirl vanes in Figures Figure 5-4 and Figure 5-5. NO generally increases with increasing center O_2 flow rate and increasing secondary CO_2 flow rate. However, there was a minimum in energy specific NO at 4.7 kg/h center O_2 flow rate for 20 and 40 kg/h CO_2.

The flow structure with the 40° swirl vane was more complex that the lower swirl conditions. As evidenced by the flame images, the radial component of primary coal velocity was large enough to penetrate the secondary oxidizer and produce unburned coal particles outside of a flame zone. It is not possible to determine the impact changes in center O_2 and secondary CO_2 would have on mixing between the two streams and the subsequent impact on NO. As noted earlier, however, the NO data all correlate fairly well with swirl number.

52
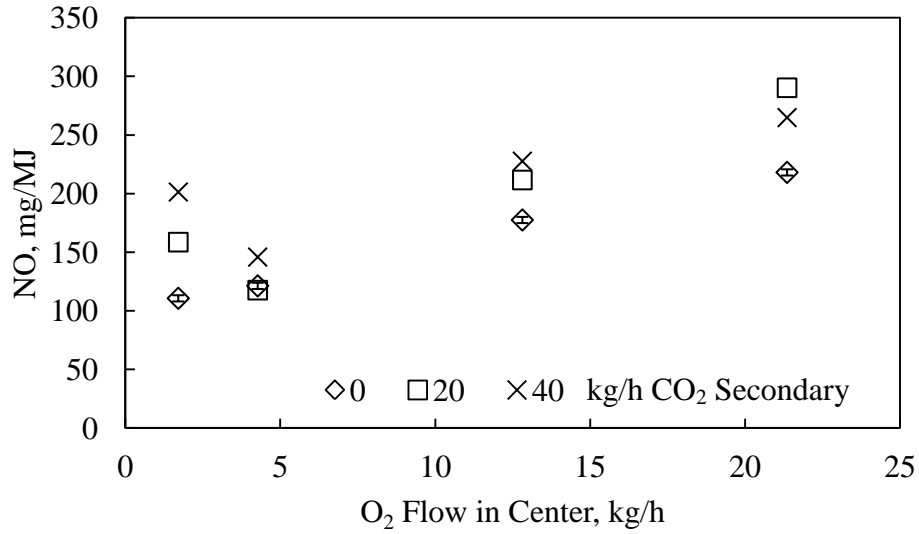
Figure 5-6: Effect of O$_2$ location and CO$_2$ dilution on energy specific NO with 40° swirl with maximum error shown with 0 kg/h CO$_2$.

5.2.5 NO Conclusions

The NO results can be explained by oxygen entrainment within the near-burner recirculation zone. Energy specific NO formation was found to correlate with swirl number, decreasing with increasing swirl. Increasing center O$_2$ flow rate improved flame stability but increased oxygen availability in the fuel rich region and increased NO formation, in agreement with studies done by Nikzat et al. [36] and Hu et al. [35]. Increasing secondary CO$_2$ flow rate increased flame lift-off length and entrainment which also increased oxygen availability in the fuel rich region and increased NO formation.

5.3 Burnout Measurements

5.3.1 Carbon Burnout as a Function of Overall Burner Swirl Number

Figure 5-7 shows the percent of carbon burnout as a function of swirl number for the 15° and 40° swirl vane data. The data from no swirl vane will be shown separately. These data show

a relatively weak dependence of carbon burnout on swirl. The burnout is relatively constant except at very low swirl. At low swirl numbers there is an increase in burnout with increasing swirl. The circled data points indicate conditions without CO_2 in the secondary stream. The data show that the addition of CO_2 to the secondary was more influential than swirl on burnout. It is difficult to attribute the effect of increasing burnout with the addition of CO_2 to a chemical effect, such as gasification reactions between CO_2 and char. This is because CO_2 is used to convey the coal to the burner for all of the operating conditions and therefore CO_2 is always available. Another possibility is that the increased lift-off length from higher CO_2 flow previously discussed may cause entrainment of O_2 which enhances oxidation of the char particles.
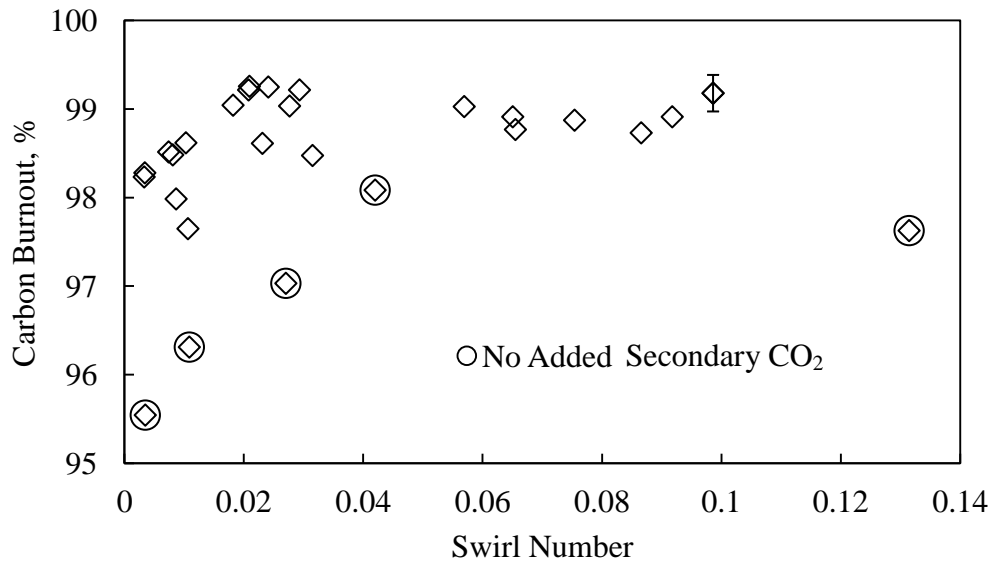
Figure 5-7: Effect of swirl number on burnout with maximum error shown on one data point.

5.3.2 Impact of Center O_2 Flow Rate and Secondary CO_2 flow Rate on Burnout, No Swirl Plate

Figure 5-8 shows the burnout data with no swirl plate as a function of center O_2 flow rate and secondary CO_2 flow rate. Burnout is fairly constant up to 12.8 kg/h center O_2 flow, and then burnout decreases with increasing center O_2 flow. The addition of O_2 should promote burnout, but at the highest O_2 flow rates burnout is reduced. One explanation for the burnout trend with increasing center O_2 flow rates is that small amounts of O_2 flow increase O_2 availability but larger flow rates transport large particles rapidly through the reactor to the exit and reduce residence time. Figure 4-3 shows velocity of the center tube for some conditions is nearly two orders of magnitude higher than the secondary flow. Figure 5-8 also shows that the burnout increases with increasing secondary CO_2 flow rate. As noted above, this may be the result of increased flame lift-off and the associated entrainment of oxidizer into the primary fuel stream.
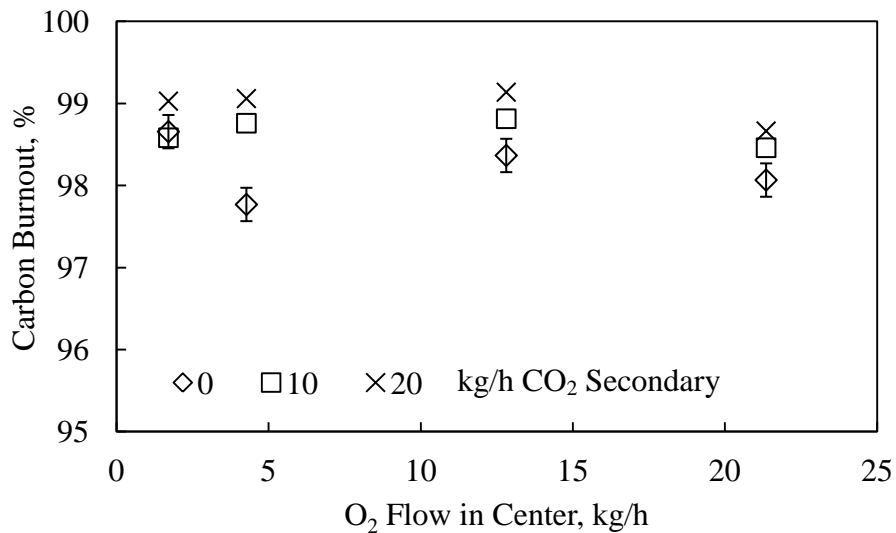
Figure 5-8: Effect of O_2 location and CO_2 dilution on carbon burnout without swirl with maximum error shown with 0 kg/h CO_2.

5.3.3 Impact of Center O_2 Flow Rate and Secondary CO_2 flow Rate on Burnout, 15° and 40° Swirl Plates

Although at different swirls, the data shown in Figure 5-7 were not a strong function of swirl, and therefore have been grouped and plotted as were the zero swirl data. Figures Figure 5-9 and Figure 5-10 show burnout as a function of center O_2 flow rate and secondary CO_2 flow rate using the 15° and 40° swirl vanes. These data show similar trends as the zero swirl vane data. Increasing CO_2 flow from 0 to 20 kg/hr increased burnout with no measurable difference between 20 and 40 kg/hr flow rates. A maximum burnout as a function of O_2 flow rate is also apparent. Burnout is maximum at 4.7 kg/hr. The burnout may change for the same reasons discussed above for the data taken without swirl. Increasing CO_2 flow rate increased entrainment and mixing between the primary and secondary streams. Also, a small amount of center O_2 flow is beneficial to burnout, but too much causes jet-entrained particles to have reduced residence time and reduced burnout.
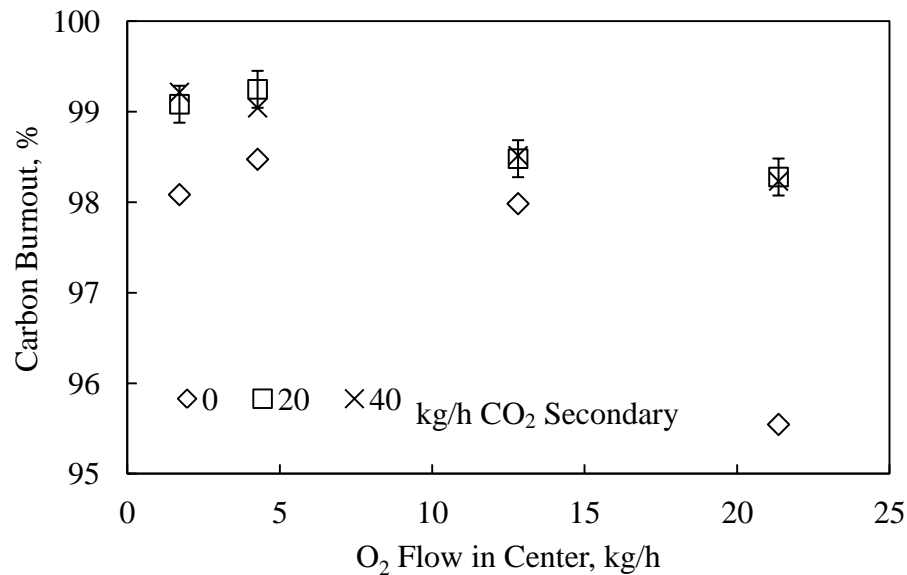
Figure 5-9: Effect of O_2 location and CO_2 dilution on burnout with 15° swirl with maximum error shown with 20 kg/h CO_2.

56
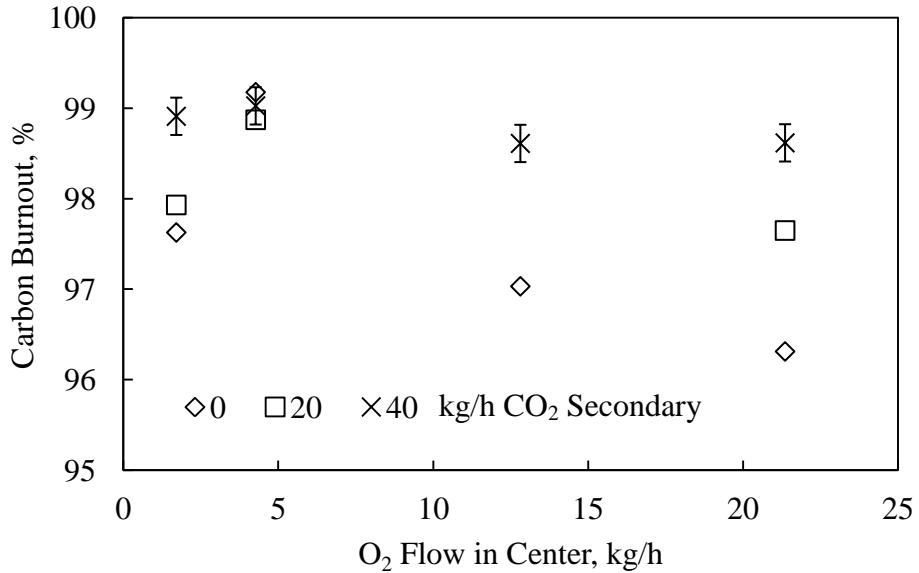
Figure 5-10: Effect of O₂ location and CO₂ dilution on burnout with 40° swirl with maximum error shown with 40 kg/h CO₂.

5.3.4 Burnout Conclusions

Burnout increased with increasing secondary CO_2 flow rate because of mixing and entrainment of secondary O_2 into the primary stream. Burnout also increased with increasing center O_2 flow, but decreased when the center stream entrained coal particles and reduced the residence time. There is no strong trend between burnout and swirl.

Although the correlation exists between increasing secondary CO_2 flow rate and increased burnout, the increase cannot be attributed to gasification reactions because the primary stream uses CO_2 to convey the coal making CO_2 present in all flow conditions. Further investigation is needed to determine if gasification reactions are significant in this combustion environment.

6 PETROLEUM COKE RESULTS

Table 6-1 summarizes the four operating conditions and resulting energy specific NO, temperature, and emissivity data measured for petcoke. In Table 6-1, "P" stands for primary, "C" stands for center, and "S" stands for secondary.
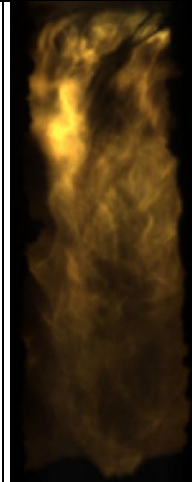
Table 6-1: Results for petcoke. Abbreviation in this table are: Primary (P), Secondary (S), and Center (C).

Condition	Air P, kg/h	O_2 C, kg/h	O_2 S, kg/h	CO_2 S, kg/h	Swirl Number	NO, mg/MJ	Temp, K	Emissivity
1	21.7	4	37	40	0.492	240	1839	0.531
2	21.7	20.5	20.5	10	0.153	220	1953	0.454
3	21.7	20.5	20.5	0	0.106	285	2093	0.413
4	30	4	35	0	0.411	405	1968	0.453

Visual attributes of the flame were recorded qualitatively including images shown in Table 6-2. Conditions 1 and 4 were similar: both flames were lifted from the burner to a distance of about 10 cm, and they were both more than twice as long as conditions 2 and 3. Conditions 2 and 3 both produced attached flames, and the only common factor between conditions 2 and 3 that differs from conditions 1 and 4 was that conditions 2 and 3 had higher center O_2 flow rates. This demonstrates that O_2 addition into the fuel rich region along with swirl was necessary to attach a petroleum coke flame. Pictures of these conditions are shown in Table 6-2, with liftoff evident for conditions 1 and 4. Visual flame intensity between the conditions in Table 6-2 can be

estimated qualitatively if exposure times are considered. If the exposure time is low, then the flame was more intense. For example, condition 3 had the lowest exposure time, and therefore the brightest flame, while condition 1 was the least intense.

Table 6-2: Representative images of petcoke flames flames for conditions specified in Table 6-1.

Condition	1	2	3	4
Exposure Time, ms	0.167	0.067	0.032	0.05
Flame Image				

6.1 Temperature and Emissivity Measurements for Petroleum Coke

Figure 6-1 shows temperature and emissivity as a function of total diluent flow into the BFR. Diluents included the sum of secondary CO_2 and primary air N_2. As diluent flow into the BFR increased, temperature decreased and emissivity increased. The data show opposite trends for temperature and emissivity. The flame of highest temperature had the lowest emissivity.

Temperature dependencies can be explained for the petcoke results using the same principles discussed with the coal flame by Draper [1]. Adding cold diluent into a reaction will lower the adiabatic flame temperature. This trend is seen in Figure 6-1. Draper [1] also reported that temperature and emissivity will tend to have opposite trends: as temperature decreases,

emissivity will increase and vice versa. In the petcoke data, the flames with lower emissivity have higher center O_2 flow rates or additional air in the primary stream which would tend to produce lower concentrations of soot as expected.
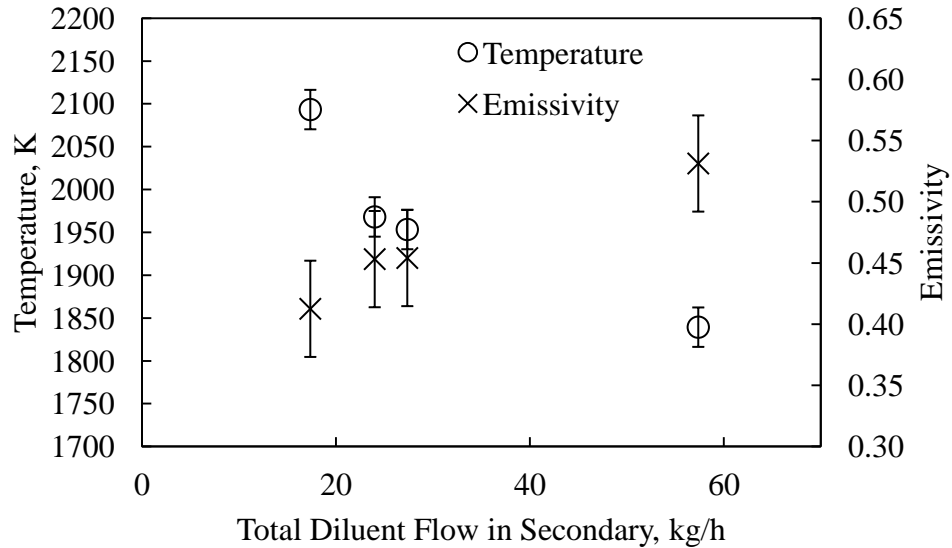
Figure 6-1: Temperature and emissivity as a function of total diluent ($CO_2 + N_2$) flow with maximum error.

6.2   NO Measurements for Petroleum Coke

Figure 6-2 shows energy specific NO measured as a function of the total N_2 flow in the primary. Conditions 1, 2, and 3 are all within 45 mg/MJ of NO, and are therefore similar in magnitude. However, condition 4 was significantly different than the others being 120 mg/MJ more NO than condition 3. Since a systematic parametric study was not conducted, it is difficult to identify the influence of a single burner operating parameter on NO. Petcoke has a low volatile yield reducing the influence of the recirculation zone on NO reduction. Instead, char NO formation and thermal NO are expected to have a more significant impact. The NO emissions

produced did not correlate well with the measured flame temperature. For example, the highest

flame temperature was recorded for condition 3 but the highest NO was produced at condition 4.

Therefore, thermal NO does not appear to be a dominant factor in the petcoke NO formation.

Char NO formation would tend to scale with oxygen availability at the particle surface.

Total O_2 flow rate was constant for all four operating conditions, but conditions 1 and 2 had

added CO_2 which decreased overall O_2 concentration. These two operating conditions do have

the lowest NO emissions. Furthermore, the local concentration at the particle surface should be

of more importance than the overall concentration. Although condition 3 had the highest overall

oxygen to diluent ratio, the images showed that the added air flow of condition 4 produced a

lifted flame. This indicates increased oxygen entrainment prior to ignition and may indicate

higher local oxygen concentrations were present for condition 4 char particles. This discussion is

however speculative and would require additional data to be more conclusive.
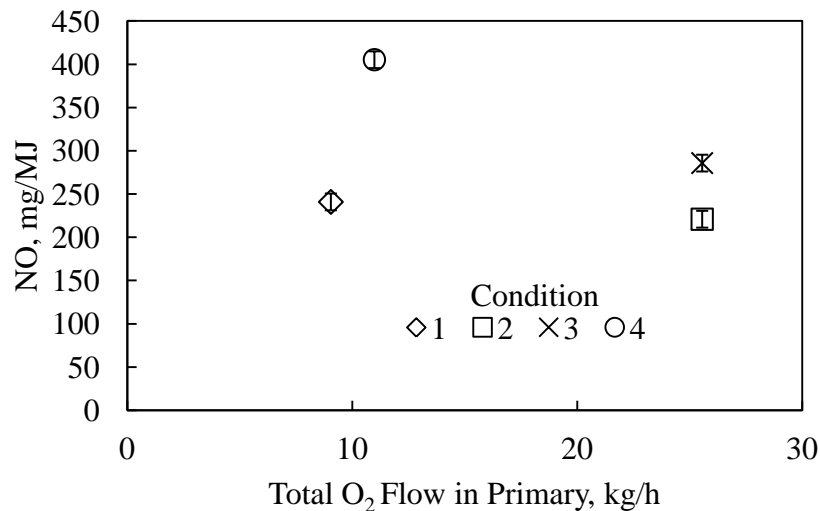
Figure 6-2: Energy specific NO as a function of N_2 flow with maximum error.

6.3 Petroleum Coke Conclusions

Due to the low reactivity of petroleum coke compared to coal, strategic locations of O_2 addition were investigated. These included adding swirl into the secondary as well as the primary and using air to convey the fuel in the primary stream rather than CO_2. These changes caused large increases in swirl numbers, and also increased the turbulence of the flame. Flame lift-off decreased when center O_2 flow rate increased. Temperature decreased and emissivity increased with increasing diluent flow. NO emissions were not correlated well with temperature indicating thermal NO was no the dominant mechanism for NO formation.

7 TOTAL HEAT FLUX AND TWO-COLOR IMAGING FOR AIR- AND OXY-COAL FLAMES

This chapter is a version of a paper submitted to the 37th International Technical Conference on Clean Coal and Fuel Systems in Clearwater, Florida [44] revised for insertion into this thesis.

7.1 Introduction

One of the major concerns in the design of a coal-fired boiler is the need to match heat flux with the desired profile needed to produce steam for power generation. Oxy-coal combustion presents new challenges and opportunities related to heat flux in comparison to air-fired combustion. Wall et al. [23] and Toftegaard [10] in their reviews of oxy-combustion discuss the primary issues involved. Heat transfer in the near-burner region of a boiler is primarily the result of radiation. The total radiative heat transfer is a function of the temperature and effective emissivity of the radiating media. The radiating media in coal combustion are spectrally radiating gases (CO_2 and H_2O) and broad band radiating particles (coal, char, ash, and soot). Oxy-coal combustion produces higher concentrations of CO_2 and H_2O and a wider range of flame temperatures compared to air-fired coal combustion. Experiments reported by Toftegaard et al. [10] and completed by Woycenko et al. [45] show a concentration of 26% O_2 in the oxidizer stream to produce a similar heat flux profile to air containing 21% O_2. Although the calculated adiabatic flame temperature of 26% O_2 in the recycle stream is lower than air

combustion, the increased emissivity of CO_2 and H_2O were reported to make up the difference. This type of empirical result cannot, however, be applied to all oxy-coal flames. Soot and radiating particles can play a dominant role in coal flame radiative heat transfer [46], and it has been shown that the recycle flow rates impacts burner flow dynamics which impact the amount of soot formation [47, 48]. Andersson et al. [47] measured total heat flux and modeled soot formation and particle radiation for propane and lignite with air and oxy-flue gas as oxidant. They concluded that the emission from soot created by the recycled flow conditions produced the largest differences between air and oxy-fired flames and was more significant than differences in CO_2 and H_2O concentrations. Their model predicted that soot radiation normally dominates over gas radiation except under wet oxy-fired recycle conditions when particle scattering is considered. In this case gas and particle radiation are similar. It is therefore important to understand the relative magnitudes of particle and gas emissions as well as the impact that flame size and shape may have on the relative amounts of heat transfer.

7.2 Objective

The objective of this work is to compare total radiative intensity profiles for air and oxy-fired coal flames of various oxidizer oxygen concentrations. Measurements included time-averaged, narrow angle radiometry and high speed imaging of the flame along the same line of sight.

7.3 Experimental Setup and Procedure

A 150 kW, down-fired, pulverized coal facility called the Burner Flow Reactor (BFR) capable of air or warm (above 211 $^\circ$C, 410 $^\circ$F) oxy-fired recycle was used to produce the coal flames. The BFR facility, shown in Figure 7-1, can be separated into three functional groups:

reactor inputs (coal, oxygen, air, and CO_2), the refractory lined water cooled reactor, and the flue gas recycle system. Coal was fed to the reactor using a bulk bag unloader and gravimetric, computer-controlled, loss-in-weight, dual auger feeder. Carbon dioxide was used to convey the coal to the burner. Carbon dioxide and oxygen were supplied from liquid Dewars. The burner was an Ijmuiden, movable block, variable-swirl type. Primary coal and CO_2 were fed into the center tube of the burner with swirled oxidizer in an outer annulus. The calculated swirl number for all cases was 0.6.

The BFR consists of six, 0.75 m diameter, 0.4 m length cylindrical sections each containing four access ports 0.150 m in width and 0.250 m in length located at 90 degree intervals around the reactor.

The exhaust system has a wet bottom barrel and cyclone for particle removal followed by a high temperature fan (315 °C, 600 °F) to recycle exhaust back to the burner. The recycled exhaust line is insulated to keep the exhaust above the acid dew point temperature and returns to the burner at approximately 210 °C (410 °F). The exhaust that is not recycled is cooled and expelled by a low temperature draft fan.
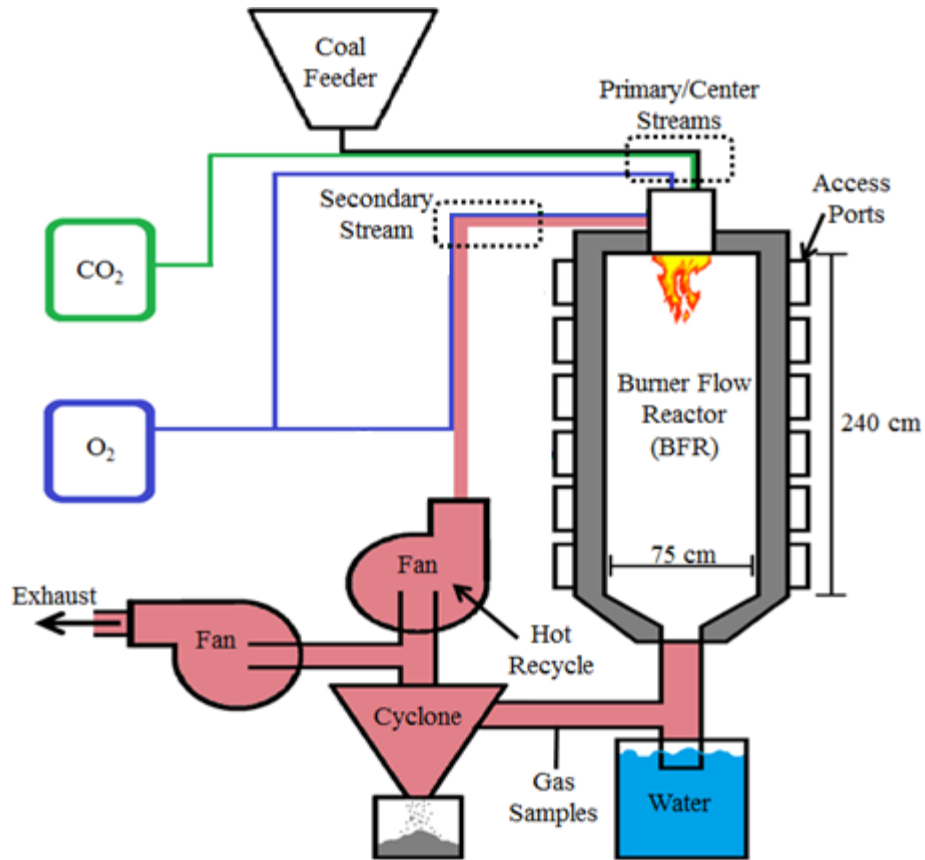
Figure 7-1: BFR system schematic with ports on BFR labeled.

The measurement of heat flux involved the use of a water-cooled narrow angle radiometer as shown in Figure 7-2. A Vatell Corperation model TG1000-30 heat flux microsensor (HFM) was located in a water cooled tube and purged with argon. The sensor housing produced a narrow viewing angle of 5.1° or 0.025 sr. The face of the sensor was painted black (emissivity 0.95) and calibrated by the manufacturer who provided and NIST traceable calibration certificate. The manufacturer reports that an incandescent lamp's irradiation was characterized using heat flux gages calibrated by insertion into a black body cavity. The cavity temperature and the lamp voltages were measured with a NIST calibrated pyrometer and voltage sources. The probe was inserted into the BFR through one of two holes in the BFR ports, as shown in Figure 7-3. The water cooled housing maintained the HFM sensor below 50 °C.

Opposite to the heat flux sensor, a water-cooled target was used to create a background with negligible emission. The sensor housing was designed to have a viewing angle that allowed the sensor to see only the target at its farthest distance in the reactor. This was confirmed by moving the target slightly from side to side and up and down while monitoring the heat flux. The heat flux did not change for these small movements indicating hot walls were not seen. However, when moving the target larger distances, the heat flux increased indicating hot walls were being seen by the HFM. Measurements were taken at five axial locations from the burner exit: two axial locations in each of the top two sections of the BFR and in the top port of the third section. Although the HFM and cold target are movable to allow for heat flux over a shorter path length to be measured, for this study both the probe tip and the target were held flush against the reactor walls for a fixed total path length of 0.75 m.
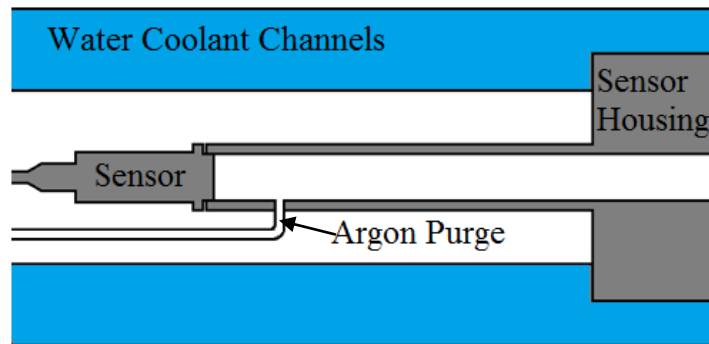
Figure 7-2: HFM heat flux sensor and probe schematic.
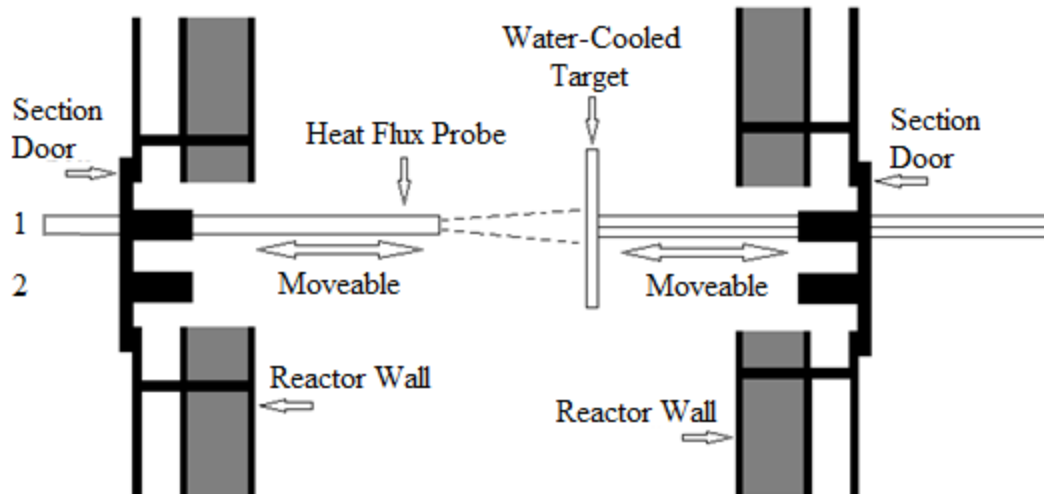
Figure 7-3: Schematic for HFM probe and target in BFR, with port holes labeled.

In addition to total radiative heat flux, band intensity measurements were obtained along the same line of sight as the total radiation measurements using a calibrated digital color camera. The camera has been used in previous experiments to measure flame temperature and emissivity. This color band method has been described in detail by Svensson et al. [46] and Draper et al. [22]. In this case, the camera captured images through the same hole that was used to insert the total radiation heat flux probe. Although the two measurements were not made simultaneously, the reactor was maintained at steady state for a given operating condition. A total of 50 images were collected from each operating condition. Variation in the image intensity was dependent on the position where the measurement was taken and is therefore difficult to characterize. Near the burner the flame was continuous and three images have been found to produce a reasonable average (Draper [1]). However, on the edge of the flame where the flame is intermittent at any instance in time, averaging of more images is desirable. A total of 10 images were used to produce the averaged values for all locations reported. As an indication of repeatability of measurements obtained from images, one of the least repeatable locations was measured twice to produce two values each averaged from 10 images. The standard deviations of temperature,

70

emissivity and total radiative intensity for this case were 1.5, 22.8 and 33.6% of the averages, respectively. These results show that temperature is very repeatable but emissivity and intensity are very dependent on the presence of the flame. In order to obtain more accurate averaged data in locations near the edge of the flame additional repetitions of a given operating condition will be required.

The color bands for the camera are in the visible region where emission from CO_2 and H_2O is negligible. The intensities obtained from the camera are therefore a result of particle emissions only while the radiation measured using the HFM is a result of all wavelengths, both visible and infrared which includes particle and gas radiation.

All data were obtained with a bituminous, Utah, Skyline coal. Proximate and ultimate analyses for the coal are shown in Table 7-1. Flow rates for the fuel and oxidizer streams are shown in Table 7-2. The coal and oxygen flow rates were constant for all tests producing a heating rate of 145 kW. The recycle flow rate was adjusted while holding oxygen flow rate constant to produce recycled gas concentrations entering the burner of 25%, 30%, and 35% O_2. Since the recycled gas contains oxygen, changing the recycle flow rate changes the total oxygen entering the reactor and the overall stoichiometric ratio (S.R.). The average O_2 concentrations considering recycle flow, incoming pure oxygen, and CO_2 flow in the primary carrier gas are listed in Table 7-3 as well as the resulting overall S.R. of the burner.

Table 7-1: Skyline coal composition

Ultimate Analysis		Proximate Analysis	
Moisture (wt. %)	3.34	Moisture (wt. %)	3.34
H (wt. %)	4.12	Ash (wt. %)	6.05
C (wt. %)	73.81	Volatile Matter (wt. %)	34.64
N (wt. %)	1.15	Fixed Carbon (wt. %)	55.97
S (wt. %)	0.90		
O (wt. %)	10.63	Higher Heating Value (Btu/lb)	13,353
Ash (wt. %)	6.05		

Three factors were found to be important in understanding the uncertainty of the total radiative HFM measurements: electrical noise, reflectance of irradiation on the coal target, and reactor repeatability. The latter two issues are considered in the measurement uncertainty not because they impact the ability of the gage to measure heat flux accurately but because impact whether the desired heat flux is produced in the experimental setup.

After grounding and insulating the HFM, the noise-to-signal ratio for the lower heat flux intensities was found to be on the order of ±5%. Ash deposition on the cold target was found reflect irradiation from the flame. The target was blown clean using compressed air between measurements to reduce the impact of this reflectance on the measured heat flux. At the location of highest ash deposition, the heat flux was found to increase 5% over a period of 15 min. By limiting the time of data collection to 15 minutes between target ash removal, the error due to reflectance is controlled to be less than ±2.5%. The repeatability of the operating condition is difficult to assess for all locations. As with the imaging data, locations on the edge of the flame will have a larger variation in heat flux from one data set to the next than locations of continuous flame. At a continuous flame location, the repeatability of measured heat flux was ±4.4%. Taking the root of the sum of the squared uncertainties produces a total uncertainty of 7.1%. This

uncertainty applies to locations where the flame is continuous and will be higher where in a location where the flame is intermittent.

Table 7-2: Operating conditions for air and oxy-fuel

Oxy-Fuel Operation Conditions With Recycle				
Coal Flow, kg/h	Secondary O_2 Flow, kg/h	Primary CO_2 Flow, kg/h	Recycled O_2 gas concentration.	Swirl Number
18.38	42.16	20	25, 30, 35	0.6
Air Operation				
Coal Flow, kg/h	Primary Air Flow, kg/h	Secondary Air Flow, kg/h	O_2 overall concentration, %	Swirl Number
18.38	20	195	20.9	0.6

Table 7-3: Operating conditions for air and oxy-fuel

Recycle O_2 Concentration (%)	Average Burner O_2 Concentration (%)	Overall Burner S.R.
25	23	1.15
30	27	1.12
35	31	1.10

7.4 Experimental Results and Discussion

As discussed above, total radiative intensity was measured at five different locations along the flame with air- and oxy-firing modes. The results are shown in Figure 7-4. In most cases, except oxy-fired, 23% oxygen, and the oxy-fired data at 75 cm, the heat flux is seen to decrease with increasing distance from the burner. A possible explanation for the increase in the oxy-fired radiative intensity between 60 and 75 cm is that it is an artifact of unsteady reactor operation. In locations where the flame was continuously present, the variation in intensity was measured to be 4.4% as discussed above; but in regions where the flame is intermittent, a change in flame length could cause much larger variations. All of the oxy-fired data at the 75 cm

73

location were taken consecutively and in a relatively short period of time, as the sensor was held in place while the oxygen concentrations were varied. It is therefore reasonable to assume that the flame was slightly elongated during the 75 cm oxy-fired heat flux measurements. The temperature data, shown in Figure 7-6, also shows this anomaly. The fact that two different instruments reported the same anomaly in the same period of time supports the speculation that unsteady operation caused an abnormally elongated flame for data taken at 75 cm, but more data would be necessary to confirm this.

The air-fired case produced the highest intensity of the all the flames, similar to the oxy-fired, 31% O_2 case and then the intensity decreased rapidly with increasing distance from the burner. This is consistent with visual observations that the air-fired flame was attached to the burner and visible luminosity remained primarily in the top 40 cm of the reactor. The visible luminous flame did not extend to axial positions beyond 60 cm; and therefore, for air, the intensity below 60 cm is attributed to emission from gas phase particles and hot ash.

The oxy-fired, 23% oxygen case produced a flame that was slightly detached from the burner and had a peak intensity at 35 cm before decreasing with increasing axial distance. Although the overall O_2 concentration is higher in this case than air, the coal is conveyed into the reactor with CO_2 which contains no oxygen. Theoretical adiabatic flame temperature of the oxy-fired, 23% O_2 case is also lower than that of air-fired coal, which would produce lower wall temperatures and slower heating of the incoming coal.

The oxy-fired, 27% case has a lower intensity than air near the burner but a higher intensity further from the burner. This flame was also detached intermittently but was ignited more rapidly (closer to the burner) than the 23% oxygen case.

The oxy-fired, 31% O_2 case produced the same intensity as the air flame near the burner but the intensity remained high at 35 cm and decreased more slowly than air or any of the other oxy-fired cases. This flame was visibly longer and less turbulent.
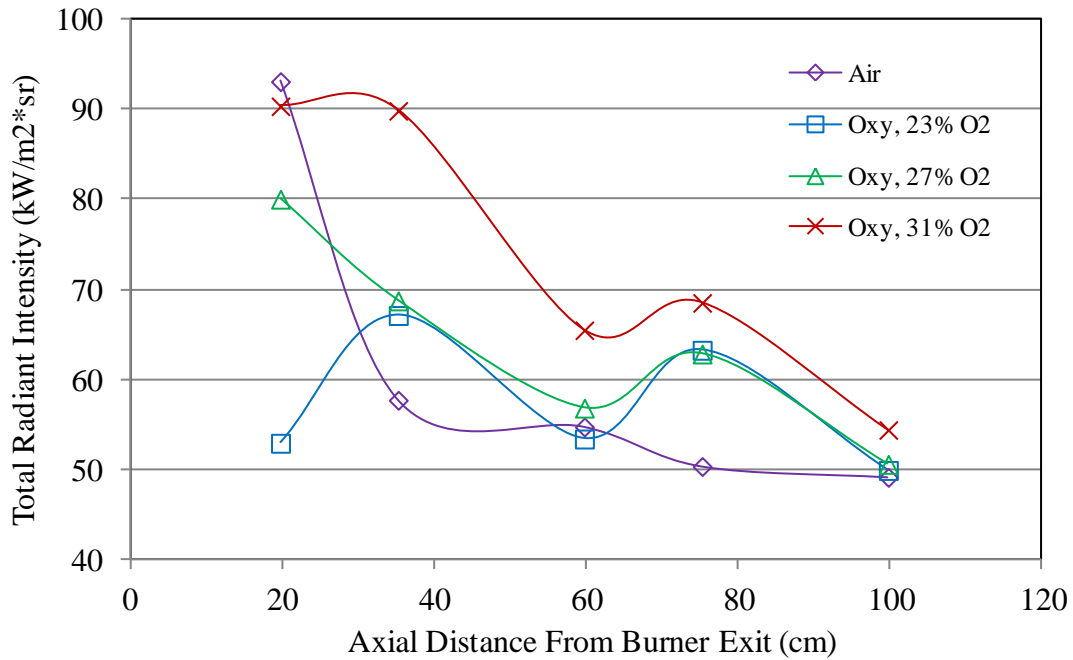
Figure 7-4: Total radiant intensity as a function of axial distance from the burner outlet.

The temperature and emissivity data obtained from the digital images of the flame provide additional evidence of the flame location and intensity. Intensity obtained from the digital image was used to calculate the temperature and emissivity of particles from the same line of sight as the total radiation intensity measurement shown in Figure 7-4. If a flame was not present during the collection of an image or filled only a portion of the image, the pixels in that portion of the image could not be used to determine the temperature of that location because of insufficient intensity. The fraction of pixels that solved and produced a temperature was used as an indication of the presence of luminous particles. Therefore, the value for pixels solved over

total pixels shows the percent of the image that contains luminous particles from the flame and is shown in Figure 7-5.

These data are similar in the trends produced of the radiant intensity although they were obtained with a completely different instrument. Evidence of a flame is clear in the top 40 cm of the reactor for all flames. The air flame luminosity ends near 60 cm while the oxy-flames extend to 75 cm. All flame luminosity high enough to be used for temperature measurement is gone by 100 cm. Since the camera only measures intensity emitted in the visible wavelengths, and radiative intensity was not large enough at 100 cm to emit radiation in those bands, temperature could not be measured. On the other hand, the heat flux sensor measures intensity from all wavelengths incident on its face, and therefore could measure irradiation from particles at this location, which included ash and large burning coal particles.

Using the images from the digital camera, the temperature and effective emissivity along the line of sight were calculated for 10 images. Only the pixels with a high enough intensity to produce a temperature and emissivity were then averaged. The results are shown in Figures Figure 7-6 and Figure 7-7. The data show a trend of decreasing flame temperature with increasing axial distance. The temperature produced by this pyrometry is heavily weighted by the temperature of soot particles on the side of the flame closest to the camera. Because the coal flame is a turbulent diffusion flame, the soot particles should be close to the stoichiometric flame temperature of the mixture. The decrease in flame temperature is therefore attributed to heat loss in the reactants that make up the flame mixture. The heat loss from the reactants increases with increasing distance from the burner.

Near the burner, at an axial distance of 20 cm, the air flame produced the highest temperature followed by oxy-fired, 23% O_2. These two operating conditions have the lowest

ratios of oxygen to diluents and therefore should produce the lowest stoichiometric adiabatic flame temperature. The fact they produced higher temperatures than the 27 and 31% O_2 conditions near the burner must be a result of the higher secondary flow rates producing flames that release more energy near the burner. As distance increases from the burner, the higher oxygen concentration flame temperatures become higher than the air and oxy-fired 23% O_2 flame temperatures as expected.

The images of the flame were captured within the same total sampling period of time as the total radiation intensity measurements shown in Figure 7-4 and show some of the same tendencies of higher radiative intensity for the oxy-fired cases at 75 cm.
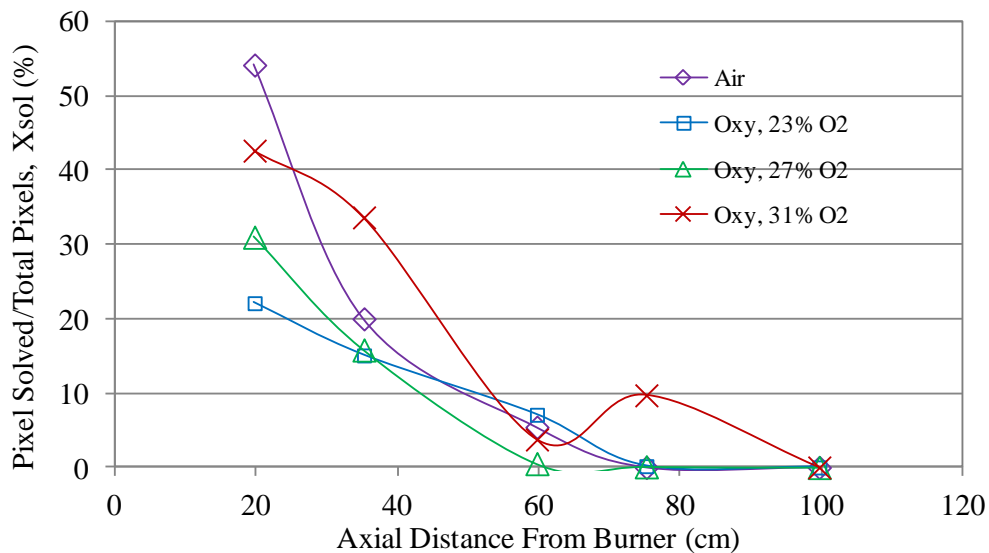
Figure 7-5: The fraction of the total number of pixels within an image that produced a measured flame temperature was used as an indication of the presence of a flame.
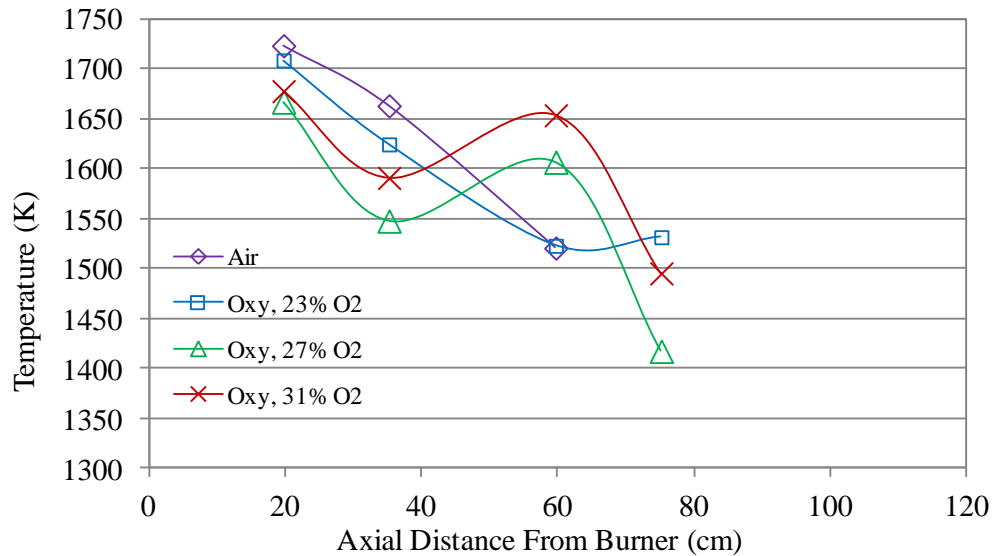
Figure 7-6: Temperature of radiating particles along a line of sight.

Emissivities were calculated by averaging all the pixels solved in 10 separate images. The emissivity generally decreases with distance from the burner. Since images were consistently obtained from the same side of a flame (in this case the side of the oxidizer) the emissivity measurements can be used as an indicator of soot concentration in the flame. The emissivity therefore indicates less soot is formed further from the burner due to increased mixing with increased axial distance from the burner. The emissivity is highest for the air-fired flame near the burner and then drops rapidly with axial distance. In the oxy-fired cases, the highest emissivities are at axial position 35 cm from the burner indicating the flame is more detached and elongated. These data suggest that the air flame has produced high soot and high temperature near the burner producing a higher heat flux. The oxy-fired flames can produce more or less soot than the air-fired flame depending on the flame structure. The long, low velocity flame produced with 31% oxygen in the recycle produces a high emissivity presumably because of low mixing and rapid ignition while the lower oxygen concentration of 23% produced less soot because of the higher flow rates of secondary oxidizer and increased mixing prior to ignition.
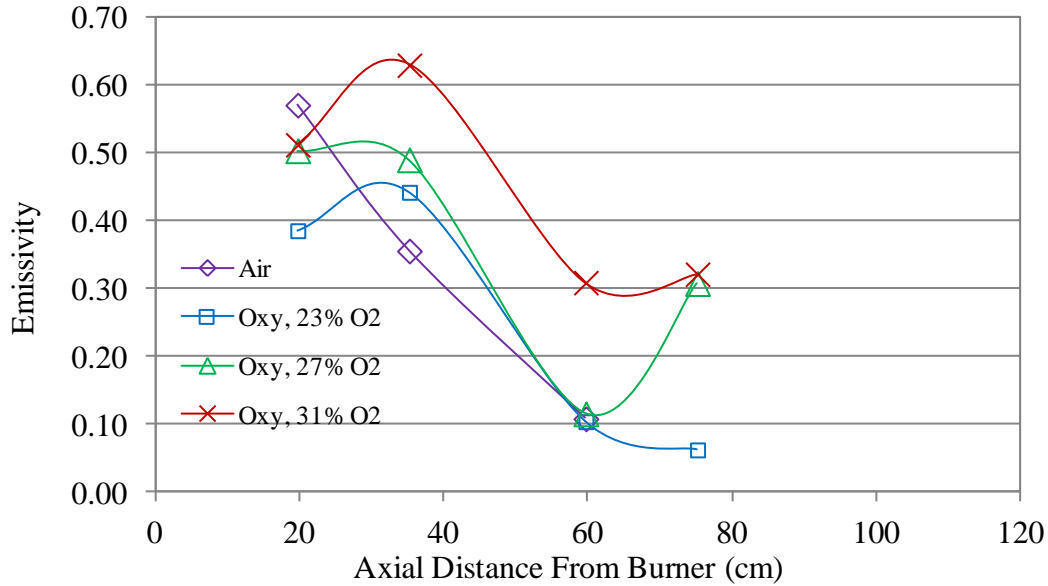
Figure 7-7: Average emissivity for all pixels solved from 10 images of air and oxy-fired flames.

The digital camera measures radiative intensity within a color band in the visible spectrum which does not include emission in the infrared where gas radiation is significant. The HFM measures total radiative intensity. It is of interest to compare the two results. In order to extend the digital camera's color band intensity to a total radiative intensity, an emissivity model valid over the entire spectrum is needed. The radiative intensity measured in the visible color bands is expected to be dominated by soot. The emissivity calculated from the flame images was determined using the Hottel and Broughton spectral emissivity model for soot as given by Equation (**7-1**. In Equation (**7-1**, KL is the optical thickness and is proportional to the soot concentration. KL is also determined independent of a wavelength as described by Draper et al. [22]. λ is the wavelength and α is the Hottel and Broughton emissivity constant. α is equal to 1.39 in the visible spectrum.

$$\varepsilon_\lambda = \exp\left(\frac{-KL}{\lambda^\alpha}\right)$$

(7-1)

In order to calculate a total intensity, the product of the spectral intensity and spectral emissivity were integrated over the entire spectrum. This required emissivity models that were valid over the entire spectral range, not just the visible wavelengths. A piecewise emissivity model was selected as indicated in the Table 7-4 below.

Table 7-4: Spectral emissivity model.

Spectral Range	Emissivity Model
0 – 400 nm	ε_λ = constant = $\varepsilon_{\lambda=400nm}$
400 nm – 750 nm	$\varepsilon_\lambda = \exp\left(\dfrac{-KL}{\lambda^\alpha}\right)$, α = 1.39
750 – 10,000 nm	$\varepsilon_\lambda = \exp\left(\dfrac{-KL}{\lambda^\alpha}\right)$, $\alpha = 0.99$

The resulting equation for total particle intensity is shown in Equation (**7-2**. In this equation, I_λ is spectral intensity and $I_{\lambda,b}$ is the blackbody spectral intensity. The result of total particle intensity obtained from the digital images is shown in Figure 7-8. The intensities are similar in magnitude and the trends are the same as the narrow angle radiometer data shown in Figure 7-4. Intensity is highest near the burner and for the oxy-fired cases, intensity increases with increasing oxygen concentrations. The radiative intensity from the particles is also seen to be slightly lower that the total intensity from the radiometer. This is to be expected because the heat flux measured with the digital camera is not sensitive to infrared radiation where gas radiation is dominant. An infrared filter was used on the camera to allow only visible light to enter the camera.

$$I_{total} = \int_0^{400} \varepsilon_{\lambda=400} I_{\lambda,b} d\lambda + \int_{400}^{750} \exp\left(\frac{-KL}{\lambda^{1.39}}\right) I_{\lambda,b} d\lambda + \int_{750}^{10,000} \exp\left(\frac{-KL}{\lambda^{0.99}}\right) I_{\lambda,b} d\lambda \qquad (7\text{-}2)$$

The camera based radiation has the advantage that the components responsible for the intensity, temperature and emissivity, can be evaluated. The disadvantage of the camera intensity method is that it is not time averaged and not well spatially averaged. The results are averaged from only the pixels in the camera where the intensity was high enough to allow the image to be processed. The low end intensities are therefore thrown out and not averaged producing a bias toward high intensity. The narrow angle radiometer is therefore the more accurate method and the camera based method must be considered semi-quantitative.
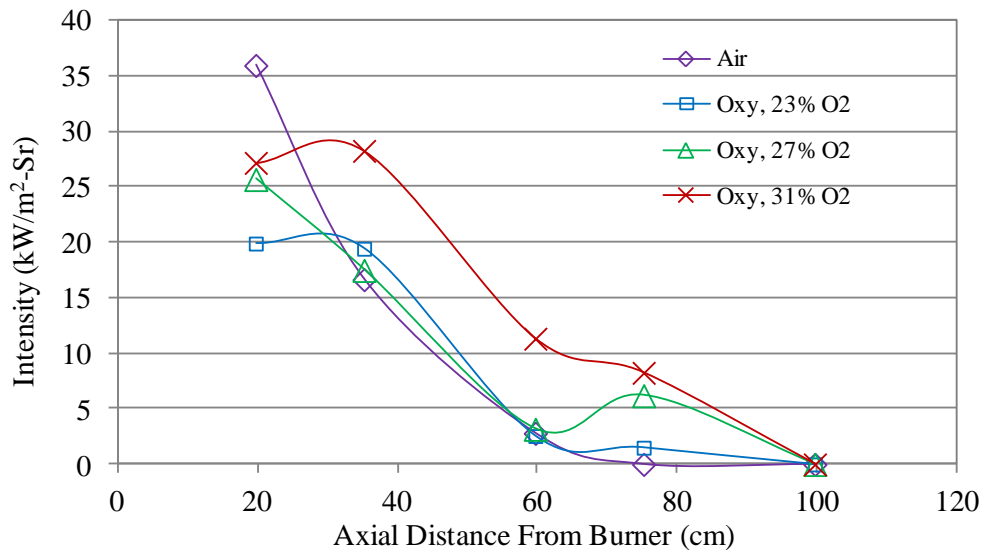
Figure 7-8: Total spectral intensity calculated from the digital images averaged over the pixels that solved in 10 images for both air and oxy-fired flames.

7.5   Conclusions

Total radiative intensity has been measured using a narrow angle radiometer in air and oxy-fired flame where the oxygen concentration in the oxy-fired flame was varied from 23 to 31%. The intensity was found to be a strong function of axial position and oxygen concentration. The air-fired flame was short and produced higher intensities near the burner than any of the oxy-fired flames. The oxy-fired, 31% O_2 flame produced higher radiative intensities for most of

the flame length. The oxy-fired 27% flame produced a lower intensity near the burner and higher intensity after 60 cm from the burner, perhaps producing the closest match to the air flame heat transfer profile. The flame images showed that soot was formed in high concentrations near the burner dominating heat transfer by particle emission but at 60 cm from the burner and downstream, intensity was dominated by gas and ash particle emissions. Increasing the amount of O_2 in the secondary by decreasing the recycle flow rate elongated the flame moving the root of the flame closer the burner and the tip further from the burner. Radiative transfer from particles was more important in the oxy-fired flames because of this increased luminous region. The highest flame temperature measured was for air at the base of the flame and then for oxy-fired 27% O_2 in the oxidizer. Increased flame temperature resulted from increased oxygen concentration in the oxy-fired flames but because they were slower to form, and lost heat prior to ignition, the air-fired flame temperature was higher near the burner base. The data show that oxy-coal combustion can change flame shape, temperature and soot concentration all of which can influence heat flux. In order to match flame temperatures, Oxy-coal flames typically have lower velocities which can reduce mixing and produce more soot. The soot tends to increase heat flux in the near burner region more that the increased CO_2 and H_2O concentrations. The increase in heat flux produced by higher CO_2 and H_2O appears modest in comparison to differences produced by particle radiation.

8   SUMMARY AND CONCLUSIONS

A novel burner developed by Air Liquide utilizing neat oxygen injection was tested for performance with regard to NO and burnout. NO, temperature and emissivity results were also collected for the same burner while burning petroleum coke. Parameters investigated included O_2 injection location, swirl number, and CO_2 flow rate. An experiment was also conducted with the BYU burner to measure heat flux comparing air and oxy combustion.

For the coal flame it was found that increasing swirl, decreasing secondary CO_2 flow rate, and increasing center O_2 injection all reduced flame liftoff from the burner producing a more stable flame. Neat O_2 injection into the center tube, however, resulted in increased NO formation. Increased secondary CO_2 injection decreased flame temperature and in most cases increased NO by causing increased oxidizer entrainment. The addition of center O_2 had a complex effect on burnout. Small additions of center O_2 flow rate improved burnout but large flow rates decreased burnout, because of decreased residence times created by the high velocity of the center O_2 jet.

The Air Liquid burner showed that high oxygen participation flames can be produced without melting the burner. Strategic oxygen injection can be used to attach and stabilize a flame but was not done without an increase in NO formation within the flame. Swirl on the other hand can stabilize the flame and decrease NO formation. Although flame temperatures were high, the NO produced could be explained by conventional low NOx burner arguments which assume fuel

NO is the dominant formation mechanism; therefore, thermal NO formation was found to be minimal in spite of the higher flame temperatures.

Petroleum coke flames showed a decrease in flame temperature with an increase in total diluent flow rate. The emissivity data showed the opposite trend, increasing with increasing diluents. The addition of center O_2 flow and the increase in swirl produced by the secondary swirl both improved flame stability and decreased flame lift-off. The addition of center oxygen did not have a large negative impact on NO emissions. The highest flame temperature did not correlate with the highest NO emissions, showing thermal NO to not be the driving force for NO formation.

Total radiant intensity axial profiles were obtained for air combustion and oxy-combustion with three combinations of O_2 mole fraction in the recirculated flue gas for oxy-combustion: 25%, 30%, and 35%. Increasing the O_2 concentration was obtained by decreasing the flow rate of the recycled flue gas, which changed the shape of the flame. The axial profile for air was highest near the burner and decreased with increasing distance from the burner. The oxy-combustion profiles began with a low flux near the burner but the intensity dropped more slowly indicating a longer flame. Lower flow rates elongated the flame because of reduced mixing. The differences in radiative profiles were caused by a combination of high O_2 concentration, which tended to produce higher temperatures, and lower flow rates, which elongated the flame and increased total radiative heat transfer.

REFERENCES

[1]   T. Draper, "Application of Two Color Pyrometry to Characterize the Two-Dimensional Temperature and Emissivity of Pulverized-Coal Oxy-Flames," BYU, Provo, 2012.

[2]   "Energy-Related Carbon Dioxide Emission," US Energy Information Administration, [Online]. Available: http://www.eia.gov/forecasts/aeo/er/early_carbonemiss.cfm. [Accessed April 2012].

[3]   "Energy," Australian Coal Association, [Online]. Available: http://www.australiancoal.com.au/energy.html. [Accessed April 2012].

[4]   "Electricity Supply, Disposition, Prices, and Emissions," US Energy Information Administration, [Online]. Available: http://www.eia.gov/oiaf/aeo/tablebrowser/#release=EARLY2012&subject=0-EARLY2012&table=8-EARLY2012&region=0-0&cases=full2011-d020911a,early2012-d121011b. [Accessed April 2012].

[5]   R.P. van der Lans, P. Glarborg, and K. Dam-Johansen, "Influence of process parameters on nitrogen oxide formation in pulverized coal burners," *Progress in Energy and Combustion Science,* vol. 23, pp. 349-377, 1997.

[6]   "EcoSmart Concrete," EcoSmart, [Online]. Available: http://ecosmartconcrete.com/. [Accessed April 2012].

[7]   "Kyoto Protocol," United Nations Framework Convention on Climate Change, [Online]. Available: http://unfccc.int/kyoto_protocol/items/2830.php. [Accessed April 2012].

[8]   Intergovernmental Panel on Climate Change, [Online]. Available: http://ipcc.ch/. [Accessed April 2012].

[9]   B.J.P. Buhre, L.K. Elliot, C.D. Sheng, R.P. Gupta, and T.F. Wall, "Oxy-fuel combustion technology for coal-fired power generation," *Progress in Energy and Combustion Science,* vol. 31, pp. 283-307, 2005.

[10] M.B. Toftegaard, J. Brix, P.A. Jensen, P. Glarborg, and A.D. Jensen, "Oxy-fuel combustion of solid fuels," *Progress in Energy and Combustion Science,* vol. 36, pp. 581-625, 2010.

[11] C.R. Shaddix and A. Molina, "Fundamental investigation of NOx formation during oxy-fuel combustion of pulverized coal," *Proceedings of the Combustion Institute,* vol. 33, pp. 1723-1730, 2011.

[12] C.R. Shaddix and A. Molina, "Effect of O2 and High CO2 Concentrations on PC Char Burning Rates during Oxy-Fuel Combustion," *Proceedings of the 33rd International Technical Conference on Coal Utilization & Fuel Systems,* p. pp ??, 2008.

[13] B. Shen, D. Liu, and H. Chen, "A Study of the Mechanism of Petroleum Coke Pyrolysis," *Developments in Chemical Engineering and Mineral Processing,* vol. 8, no. 3/4, pp. 351-358, 2000.

[14] N.S. Yuzbasi and N. Selçuk, "Air and oxy-fuel combustion behaviour of petcoke/lignite blends," *Fuel,* vol. 92, pp. 137-144, 2012.

[15] J. Chen and X. Lu, "Progress of pertoleum coke combusting in curculating fluidized bed boilers - A review and future perspectives," *Resources, Conservation and Recycling,* vol. 49, pp. 203-216, 2007.

[16] L.D. Smoot and P.J. Smith, Coal Combustion and Gasification, New York: Plenum Press, 1985.

[17] J.O.L. Wendt and O.E. Schultze, "On the Fate of Fuel Nitrogen During Coal Char Combustion," *AIChE Journal,* vol. 22, no. 1, pp. 102-110, 1976.

[18] E.G. Garijo, A.D. Jensen, and P. Glarborg, "Kinetic Study of NO Reduction over Biomass Char under Dynamic Conditions," *Energy & Fuels,* vol. 17, pp. 1429-1436, 2003.

[19] Q. Jia, D. Che, Y. Liu, and Y. Liu, "Effect of the cooling and reheating during coal pyrolysis on the conversion from char-N to NO/N2O," *Fuel Processing Technology,* 2008.

[20] J.R. Howell, R. Siegel, and M.P. Menguç, in *Thermal Radiation Heat Transfer, Fifth Edition*, Boca Raton, CRC Press, 2011.

[21] J.J. Murphy and C.R. Shaddix, "Influence of scattering and probe-volume heterogeneity on soot measurements using optical pyrometry," *Combustion and Flame,* vol. 143, pp. 1-10, 2005.

[22]   T. Draper, D. Zeltner, D. Tree, Y. Xue, and R. Tsiava, "Two-dimensional flame temperature and emissivity measurements of pulverized oxy-coal flames," *Applied Energy,* vol. 95, pp. 38-44, 2012.

[23]   T. Wall, Y. Liu, C. Spero, L. Elliott, S. Khare, R. Rathnam, F. Zeenathal, B. Moghtaderi, B. Buhre, C. Sheng, R. Gupta, T. Yamada, K. Makino, and J. Yu, "An overview on oxyfuel coal combustion - State of the art research and technology development," *Chemical Engineering Research and Design,* vol. 87, pp. 1003-1016, 2009.

[24]   E. H. Chui, A.J. Majeski, M.A. Douglas, Y. Tan, and K.V. Thamgbimuthu, "Numerical investigation of oxy-coal combustion to evaluate burner and combustion design concepts," *Energy,* vol. 29, pp. 1285-1296, 2004.

[25]   W.C. Hecker, K.M. McDonald, W. Reade, M. Swenson, and R.F. Cope, "Effects of burnout on char oxidation kinetics," *Symposium, International, on Combustion,* vol. 24, pp. 1225-1231, 1992.

[26]   R.K. Rathnam, L.K. Elliott, T.F. Wall, Y. Liu, and B. Moghtaderi, "Differences in reactivity of pulverised coal in air (O2/N2) and oxy-fuel (O2/CO2) conditions," *Fuel Processing Technology,* vol. 90, pp. 797-802, 2009.

[27]   W. Yan and Y. Liu, "Prediction and measurements of carbon combustion rate in CO2/O2 environments and its relevance to greenhouse gas recovery," *Symposium on Energy Engineering in the 21st Century,* pp. 1591-1594, 2000.

[28]   C.S. Wang, G.F. Berry, K.C. Change, and A.M. Wolsky, "Combustion of pulverized coal using waste carbon dioxide and oxygen," *Combustion and Flame,* vol. 72, pp. 301-310, 1988.

[29]   D. Alvarez, I.F. Dominguez, and A.G. Borrego, "Comparison of pulverised coal combustion performance under O2/CO2 and O2/N2 atmospheres," *International Conference on Coal Science and Technology, Okinawa, Japan,* 2005.

[30]   B. Arias, C. Pevida, F. Rubiera, and J.J. Pis, "Effect of biomass blending on coal ignition and burnout during oxy-fuel combustion," *Fuel,* vol. 87, pp. 2753-2759, 2008.

[31]   P.A. Bejarano and Y.A. Levendis, "Single-foal-particle combustion in O2/N2 and O2/CO2 environments," *Combustion and Flame,* vol. 153, pp. 270-287, 2008.

[32]   J.J. Saastamoinen, M.J. Aho, and J.P. Hämäläinen, "Pressurized Pulverized Fuel Combustion in Different Concentrations of Oxygen and Carbon Dioxide," *Energy & Fuels,* vol. 10, pp. 121-133, 1996.

[33]   A. Makino, "An approximate explicit expression for the combustion rate of a small carbon particle," *Combustion and Flame,* vol. 90, pp. 143-154, 1992.

[34]   A.G. Borrego, E. Osório, M.D. Casal, and A.C.F. Vilela, "Coal char combustion under a CO2-rich atmosphere: Implications for pulverized coal injection in a blast furnace," *Fuel Processing Technology,* vol. 89, pp. 1017-1024, 2008.

[35]   Y. Hu, S. Naito, N. Kobayashi, and M. Hasatani, "CO2, NOx, and SO2 emissions from the combustion of coal with high oxygen concentration gases," *Fuel,* vol. 79, pp. 1925-1932, 2000.

[36]   H. Nikzat, H. Kak, T. Fuse, Y. Hu, K. Ogyu, N. Kobayashi, and M. Hasatani, "Characteristics of pulverized coal burner using a high-oxygen partial pressure," *Chemical Engineering Research and Design,* vol. 82, pp. 99-104, 2004.

[37]   E. Croiset, K. Thambimuthu, and A. Palmer, "Coal combustion in O2/CO2 mixtures compared with air," *Canadian Journal of Chemical Engineering,* vol. 78, pp. 402-407, 2000.

[38]   N. Krishnamurthy, P.J. Paul, and W. Blasiak, "Studies on low-intensity oxy-fuel burner," *Proceedings of the Combustion Institute,* vol. 32, pp. 3139-3146, 2009.

[39]   L. Jia, Y. Tan, and E.J. Anthony, "Emissions of SO2 and NOx during Oxy-Fuel CFB Combustion Tests in a Mini-Circulating Fluidized Bed Combustion Reactor," *Energy & Fuels,* vol. 24, pp. 910-915, 2010.

[40]   C. Stimpson, "The Composition and Morphology of Coal Ash Deposits," Brigham Young University, Provo, Expected 2012.

[41]   T. Reeder, "Corrosion-related Gas Measurements and Analysis for a Suite of Coals in Staged Pulverized Coal Combustion," Brigham Young University, Provo, 2010.

[42]   S. Chamberlain, "Mesurement and Analysis of GasComposition in a Staged and Unstaged Oxy-fired Pulverized Coal Reactor with Warm Flue Gas Recycle," Brigham Young University, Provo, Expected 2012.

[43]   E.H. Chui, M.A. Douglas, and Y. Tan, "Modeling of oxy-fuel combustion for a western Canadian sub-bituminous coal," *Fuel,* vol. 82, pp. 1201-1210, 2003.

[44]   D. Zeltner, T. Draper, J. Thornock, D.R. Tree, and Y. Xue, "Total and Visible Radiative Heat Flux Intensity Measurements of Air- and Oxy-Coal Flames," in *37th International Technical Conference on Clean Coal and Fuel Systems*, Clearwater, Florida, USA, 2012.

[45] D.M. Woycenko, W.L. Van De Kamp, and P.A. Robert, "Combustion of Pulverized Coal in a Mixture of Oxygen and Recycled Flue Gas. Summary of the Apg Research Program," in *International Flame Research Foundation*, Ijmuiden, Netherlands, 1995.

[46] T.H. Fletcher, J. Ma, J. Rigby, B.A.L., and B.W. Webb, "Soot in Coal Combustion Systems," *Progress in Energy and Combustion Science,* vol. 23, pp. 283-301, 1997.

[47] K. Andersson, R. Johansson, F. Johnsson, and B. Leckner, "Radiation Intensity of Lignite-Fired Oxy-Fuel Flames," *Experimental Thermal and Fluid Science,* vol. 33, pp. 67-76, 2011.

[48] C.K. Stimpson, A. Fry, T. Blanc, and D.R. Tree, "Line of Sight Soot Colume Fraction Measurements in Air- and Oxy-Coal Flames," in *International Symposium for the Combustion Institute*, Warsaw, Poland, 2012.

[49] K. I. Svensson, A. J. Mackrory, M. J. Richards and D. R. Tree, "Calibration of an RGB, CCD Camera and Interpretation of its Two-Color Images for KL and Temperature," *SAE Paper,* pp. 2005-01-0648, 2005.

APPENDIX A. STANDARD OPERATING PROCEDURE FOR OXY-FUEL

**This procedure should be used with the Air Liquide burner. If this procedure is used with the

BYU burner or other configurations, serious damage or injury could occur. ***

8.1 Start-up

1. Check O_2/CO_2 tank levels
2. Check door gasket availability
3. Replace top east port on BFR with ignition port
4. Remove a bottom door (or can take insulation out that was used to plug a large port hole)
5. Check burner components for any melting or damage
6. Check that burner is assembled correctly
7. Check lines going to burner
   a. Coal line ball valve closed
   b. Secondary air ball valve open
   c. 3-way O_2 valve correctly oriented
   d. Methane ball valve open
8. Turn on Ingersoll Rand Compressor in B-38
9. Make sure fans are on (Breakers 29,31,33 in Panel A and 14 in Panel BA – they should be flipped to "ON")
10. Turn on the heater for the secondary air line (breaker 8 in Panel CA on the far north wall – it should be flipped to "ON")
    (Note: While the heaters are warming up, the overtemp control might throw the safety switch, cutting off power to the heater. If the red alarm LED turns on for the OVERTEMP control panel, flip down the cover and push the reset button. The OVERTEMP control is the southernmost panel on the dividing wall with the other user controls.)
11. Turn on main control panel (turn the key)
12. Turn on O_2 sensors
13. Make sure switch next to GC computer is set to "Oxy" and not "Air"
14. Make sure Oxy Emergency Shut Down Switch (next to GC computer) is switched up
15. Short the low pressure switches on the O_2 and CO_2 lines
16. Pressurize O_2 line

a. Prop open door in O_2 room that opens to outside. If there is a leak, this is the only fast way to flush out the room.
b. Attach tank using Teflon tape to connect hose to Liquid port on tank – typically, have two tanks connected
c. Make sure pressure in tank is between 100-325 psi – if too low, turn green regulator on tank a couple turns open; if too high, stand aside and open the "Vent" valve on the tank until the pressure drops to a reasonable value.
d. Open lower needle valve on vaporizer
e. Open tank valve – note: pressure gauge upstream of regulator should read the same as the pressure gauge on the tank
f. Make sure regulator is closed
g. Open ball valve upstream of one of the regulators. Only need to use one of the parallel lines.
h. Open ball valve downstream of bottom regulator
i. Open regulator until pressure gauge downstream of regulator reads 80 psi

17. Pressurize CO_2 line
a. Attach tank using gasket to connect hose to Liquid port on tank – typically, have two tanks connected
b. Make sure pressure in tank is between 100-325 psi – if too low, turn green regulator on tank a couple turns open; if too high, stand aside and open the "Vent" valve on the tank until the pressure drops to a reasonable value.
c. Switch heater power source on wall to "On"
d. Make sure heater is set to "On" and that TC is about 70°F and that LT is about 0°F
e. Open lower needle valve on evaporator
f. Open tank valve – note: pressure gauge upstream of regulator should read the same as the pressure gauge on the tank
g. Make sure regulator is closed
h. Open ball valve upstream of one of the regulators
i. Open ball valve downstream of top regulator
j. Open regulator until pressure gauge downstream of regulator reads 80 psi

18. Open all ball valves (3 on each) on both CO_2 and O_2 lines
19. Un-short the low pressure switches on the O_2 and CO_2 lines
20. Turn on exhaust fan and cooling systems (water jacket, scrubber, quench) at main control panel and window air to clear windows
21. Visually confirm that the all water coolant systems are flowing
22. Make sure that the ash barrel is connected and sealed to the cyclone
23. Pressurize secondary air stream to 50 psi
a. Open secondary air ball valve upstairs north of the reactor (high pressure air, orange line – ball valve with the long handle)
b. Close valve above pressure gauge in user control area
c. Push "Load" until pressure is 40 psi – note: if no response, push yellow wire end to empty connection spot and try again
24. Open Labview (program name is BFR2010_Darrel) and start running the program.

25. Adjust exhaust O_2 sensor with little screwdriver to read 20.9 if 15 minutes has passed and the reading is steady. Drift WILL occur if not enough time has been given for it to steady out.
26. Calibrate recycle O_2 sensors in LabVIEW
    a. Make sure "Oxy" switch is set instead of "Air"
    b. Go to "O2 Concentrations" tab, enter 20.85 for the reference value, and hit "Calibrate". Wait a few moments to get a good average reading, then hit the same button again.
27. Light reactor with methane
    a. Open Green methane ball valve on North wall near reactor
    b. Open ignition rotameter on North wall near reactor
    c. Enter the desired O_2 and CO_2 flow rates into Labview (see below for rates) but do not push "Start".
    d. Person 1 lights propane torch
    e. Person 2 is behind the safety wall and holds down ignition button
    f. Person 1 lights the methane wand from the propane torch and sticks it through the top ignition port hole. Once lit ignition wand is inside the reactor, person 1 get behind safety wall
    g. Once Person 1 is behind the wall, Person 2 flips the methane switch, while still holding down the ignition button and monitoring that the flame is still there
        Note: If flame doesn't start immediately when methane switch is flipped, turn off methane and let go of ignition and start over. Make sure to wait until the O_2 exhaust sensor reads close to 21% before attempting again.
    h. Person 2 starts O_2 and CO_2 flowing into the reactor as soon as the flame is lit
        i. Secondary Air: 40 psi
        ii. Methane: 325 SCFH
        iii. O_2P: 10 kg/hr
        iv. O_2S: 10 kg/hr
        v. CO_2P: 0 kg/hr
        Note: To update gas flow rates in LabVIEW, make sure the button on the left is switched to "Oxy" instead of "Air". Just entering the numbers into the set point fields will NOT update the controllers. The "Update Set Points" button must be pushed. The controllers will immediately update, despite any delay on the LabVIEW interface.
    i. CO_2S: 20 kg/hr
    j. If flame is lit, person 1 lets go of the ignition button
    k. Flow rates (suggested with Air Liquide burner with no secondary swirl):
    l. Monitor O_2 concentration in the exhaust to determine stoichiometry. Adjust flows accordingly. With the reactor pressure still negative, there should be about 4/5% O_2 in the exhaust.
        Note: 325 SCFH Methane is not absolute. The user can adjust flows if desired.
28. Turn off ignition switch
29. Turn off ignition rotameter
30. Turn off propane torch
31. Take methane wand out of reactor and put back – be careful 'cause it's HOT
32. Take out ignition port from top, west port and put normal door on it

33. Put south, bottom door on (or replug hole)
34. Make reactor pressure negative. Both the screw handle gate valve on the main floor and the push handle gate valve off the scrubber will control reactor pressure.
35. Adjust flow rates so that the exhaust O_2 reads about 2%
36. Start preparing instrumentation to collect data:
    a. Check GC calibration with air
    b. Start warming up Horiba
    c. Get FTIR running
    d. Get camera set up
    e. Get heat flux gauge set up
37. Monitor pressure on O_2 and CO_2 tanks.
    a. If starting to drop without being empty, open pressure build regulator valves on the tank.
        i. If tanks are full, open valves about 2 full turns. As the tanks get empty, more turns are required.

8.2   Switching from Methane to Coal

1. Once most of the reactor temperatures are above 1000 K, it is safe to switch to coal
2. To start recording information on LabVIEW, select the folder and file you wish to record in, the time interval to record, and push the "Record Data" button.
    Note: If the LabVIEW program is hard stopped (the stop sign button or CNTL+.) all data will be lost. The "Stop or Write File" button must be pushed to record the data.
3. Turn on air pressure to the feeder to 100 psi with the regulator on the wall north of the BFR
4. In the fuel room, turn switch on coal feeder to "ON" and push "Reset"
5. Check the oil level on vibrators
    a. If less than full, fill them
6. Empty water trap on vibrator air line
7. Turn on the vibrators using ball valve behind feeder – pressure should be about 20 psi
8. Turn off methane and O_2 at the same time but keep CO_2 running to keep burner cool. Do this by switching off the Methane switch on the control panel, and updating the O_2 and CO_2 set points in LabVIEW
9. Unload secondary air
    a. Open valve
    b. Push "Unload" until pressure is 0 psi
10. Switch ball valves at top of the reactor to prepare for coal
    a. Coal line ball valve open
    b. Secondary air ball valve closed
    c. 3-way O_2 valve correctly oriented
    d. Both methane ball valves closed
11. Turn on coal, O_2 and CO_2 at the same time
    a. Flow rates:
        i. Coal: 8 kg/hr

    ii. O_2P: 15 kg/hr
   iii. O_2S: 15 kg/hr
    iv. CO_2P: 20 kg/hr
     v. CO_2S: 20 kg/hr

Note: Residual coal may be left in the line. It is common for a large portion of coal to be thrown into the reactor when CO_2P starts flowing. Make sure all people are clear from the BFR vicinity when coal is started.

12. After a few moments, adjust flow rates to desired setting.
13. Open pressure in BFR
14. Close green methane ball valve on north wall near reactor
15. Turn air heater off (Breaker #8 Panel CA in far north breaker box)

8.3   Shut-Down

1. Turn off coal and O_2, but keep CO_2 running to keep burner cool
   a. Flow rates:
      i. Coal: 0 kg/hr
      ii. O_2P: 0 kg/hr
      iii. O_2S: 0 kg/hr
      iv. CO_2P: 0 kg/hr
      v. CO_2S: 40 kg/hr
2. In the fuel room, turn switch on coal feeder to "OFF"
3. Turn off vibrators
4. Stop feeder supply air with valves on wall north of the BFR
5. De-pressurize O_2 line
   a. Short low pressure switch
   b. Close valve on tank
   c. Run a small flow rate of O_2 into the reactor, watching pressure gauges on valve train until they read zero – once they hit zero, set flow rates back to zero
   d. Close the three ball valves on the O_2 valve train
   e. Close lower needle valves on vaporizer
   f. Close green regulator on tank to prevent pressure build
   g. Close ball valves upstream and downstream of bottom regulator(top regulator broken)
   h. Unscrew regulator counterclockwise a couple turns
6. Open secondary air ball valves upstairs
7. Load secondary air to 50 psi
8. De-pressurize CO_2 line but leave secondary air on
   a. Short low pressure switch
   b. Close valve on tank
   c. Run a small flow rate of CO_2 into the reactor, watching pressure gauges on valve train until the go to zero – once they hit zero, set flow rates back to zero
   d. Close the three ball valves on the CO_2 valve train
   e. Close lower needle valves on heater

  f. Close green regulator on tank to decrease tank pressure
  g. Close ball valves upstream and downstream of top regulator
  h. Unscrew regulator counterclockwise a couple turns
  i. Set heater power source on wall to "Off"

9. Adjust ball valves on second floor
  a. Coal line ball valve closed
  b. Secondary air ball valve open
  c. 3-way O_2 valve correctly oriented
  d. Both methane ball valves closed

10. Remove top door on reactor
11. Make reactor pressure negative to suck in room air, but make sure scrubber water is still running
12. Flip Oxy Main Shutdown switch downwards – this puts air running through the primary section of the burner as well
13. Turn off any instruments used (FTIR, Horiba – leave GC running, make sure the Argon pressure is at 80 psi)
14. Turn off Labview program by pushing "Stop or Write File" – **do NOT push the stop sign symbol on the upper left side of the screen, this erases all the data!** – run program again so that the reactor temperatures can still be monitored
15. Turn off O_2 sensor
16. Make sure all water cooling systems and exhaust fan are still running

Once reactor temperatures reach 400 K:

17. Turn off cooling systems and exhaust fan
18. Unload secondary air to 0 psi
19. Close secondary air main ball valve upstairs